Coupling nickel chemical speciation and isotope ratios to decipher nickel dynamics in the Rinorea cf. bengalensis-soil system in Malaysian Borneo

I. Zelano, C. Cloquet, A. van Der Ent, G. Echevarria, R. Gley, G. Landrot, S. Pollastri, F. Fraysse, Emmanuelle Montargès-Pelletier

Coupling nickel chemical speciation and isotope ratios to decipher nickel dynamics in the *Rinorea* cf. *bengalensis*-soil system in Malaysian Borneo

[1,2*]Zelano, I.O., [1]Cloquet, C., [3]van der Ent A., [4]Echevarria, G., [2]Gley R., [5]Landrot G., [6]Pollastri S., [2]Fraysse F., [2]Montargès-Pelletier, E.

[1]CRPG, UMR 7358, CNRS Université de Lorraine, 15 rue Notre-Dame-des-Pauvres, BP20, 54501, Vandœuvre-lès-Nancy, France.

[2]LIEC, UMR 7360, CNRS Université de Lorraine, 15 avenue du Charmois, 54500, Vandœuvre- lès-Nancy, France.

[3]Sustainable Minerals Institute, The University of Queensland, St Lucia, QLD 4072, Australia

[4]LSE, UMR 1120 INRA Université de Lorraine, 2 avenue de la Forêt de Haye, 54500 Vandœuvre-lès-Nancy, France.

[5]Synchrotron SOLEIL, CEA CNRS, l'Orme des Merisiers, Saint Aubin BP 48, 91192 Gif sur Yvette Cedex, France.

[6]CERIC - ERIC, Strada Statale 14, Basovizza, 34149 Trieste, Italia

***correspondence: isabella.zelano@unil.ch**

Abstract

Aims. *Rinorea* cf. *bengalensis* is a Ni hyperaccumulator which occurs in Sabah (Malaysia), on Borneo Island, that is able to accumulate considerable amounts of Ni and influences the Ni cycle in surface soil layers, both in terms of Ni concentration and Ni isotopic composition. In this study, the biogeochemical processes underpinning Ni isotopic fractionation in the soil-plant system and the mechanisms regulating Ni homeostasis in *R.* cf. *bengalensis* plants were elucidated.

Methods. Two specimens of *R.* cf. *bengalensis* of different ages and associated surface soils were collected from ultramafic soils in Sabah. Soil mineralogy, Ni concentrations, speciation and isotopic signatures were subsequently determined in plant and soil samples.

Results. Nickel in *R.* cf. *bengalensis* leaves is mainly complexed with citrate. Soil Ni available fractions have different δ^{60}Ni values depending on the Ni bearing phases. *Rinorea* cf. *bengalensis* specimens take up lighter Ni isotopes and a pronounced isotopic fractionation within the plant is observed, especially in the young specimen.

Conclusions. The results suggest that the observed fractionation in the young plant can be attributable to kinetic effects (lighter isotopes move faster), which become less evident in the older specimen, as Ni is redistributed and homogenized through phloem loading and unloading processes.

Keywords: **Ni, ultramafic soil, hyperaccumulator plants, isotopic fractionation, chemical speciation**

Introduction

Ultramafic rocks are mantle rocks characterized by a specific composition with low silica, high contents of mafic minerals (Fe and Mg oxides). Soils derived from the alteration of ultramafic rocks pose edaphic stresses for vegetation, including a low Ca/Mg ratio, lack of essential nutrients such N, P, and K, and a high concentrations of Mn, Ni, Cr and Co (Whittaker 1954; Bonifacio et al. 1997; Becquer et al. 2006). These soils are known for their hosting adapted vegetation, which includes the occurrence of hyperaccumulator plants that can achieve extraordinary levels of metal accumulation due to enhanced uptake and translocation mechanisms from the roots to the shoots (Baker, 1981). On ultramafic soils developed from serpentinized ultramafic rocks (which represent the most important terrestrial Ni reservoirs), numerous Ni hyperaccumulator plant species have been reported over the past 40 years (Reeves et al. 2018a). Hyperaccumulators can attain exceptionally high concentrations of Ni in their living tissues, with up to several weight percent Ni (*e.g.* 25 Wt% in latex or 16 Wt% in phloem sap) (Jaffre et al. 1976; Baker and Brooks 1988; Reeves 2003; van der Ent et al. 2013; Mesjasz-Przybylowicz et al. 2015; Reeves et al. 2018b; Jaffré et al. 2018). Nickel hyperaccumulator plants are known to transfer most of the Ni into their aerial parts (shoots) of the plant, instead of using root sequestration for metal detoxification (Baker, 1981). *Via* leaf litter deposition, hyperaccumulators can increase Ni concentrations of the soil in a surface area surrounding the plant (Boyd and Martens 1998). In tropical Southeast Asia, *Rinorea* cf. *bengalensis* (Violaceae) is one of more than 40 different Ni hyperaccumulator species identified from the Malaysian state of Sabah on Borneo Island (van der Ent et al. 2018b; 2019a). *Rinorea* cf. *bengalensis* is a large tree (up to 25m tall) that contain up to 4.77 kg of Ni (van der Ent and Mulligan 2015). Substantial Ni enrichment under the canopy of *R.* cf. *bengalensis* has been reported due to the degradation of leaf litter (van der Ent et al. 2015). However, it is still an open question to what extent Ni is recycled in the natural habitat of *R.* cf. *bengalensis* through Ni uptake, leaf shedding, re-uptake of Ni from decomposed leaf litter, and the Ni release in surface soil (Nkrumah et al. 2019b, d).

The interest toward Ni cycling at the Earth's surface has rapidly increased during the last decades but only a few scientific studies have been published proposing the use of stable Ni isotopes to elucidate the biogeochemical cycle of Ni in the upper soil horizons and surface waters (Elliott and Steele 2017). The degree of Ni isotope fractionation between the different surface compartments are a practical approach to identify and characterise the Ni biogeochemical processes. In order to better understand Ni isotopic fractionation on a larger scale, in

catchments or soil-plant systems, the processes that fractionate Ni isotopes at the molecular scale need to be elucidated. Recent studies contributed to this understanding by showing Ni isotopic fractionation due to sorption onto mineral phases under laboratory controlled conditions (Wasylenki et al. 2015; Wang and Wasylenki 2017; Gueguen et al. 2018; Spivak-Birndorf et al. 2018), and due to complexation with organic acids relevant for the soil-plant system (Zelano et al. 2018). Nickel is involved in various biological reactions that might be implicated in isotopic fractionation (Cameron et al. 2009) but, to date, only few works have been focused on the impact of hyperaccumulator plant homeostasis on the Ni isotopic signature in surface soils (Deng et al. 2014; Estrade et al. 2015; Zelano et al. 2018; Ratié et al. 2019). However, isotopic fractionation of metals has been observed in higher plants and has been interpreted as a consequence of physiological processes involved in maintaining homeostasis, especially with regard to Fe (Guelke and von Blanckenburg 2007), Zn (Weiss et al. 2004; Tang et al. 2012, 2016; Deng et al. 2014; Caldelas and Weiss 2017), Cd (Imseng et al. 2018, 2019) and Cu (Jouvin et al. 2012). For example, in the case of Zn, the preferential uptake at root level of heavier or lighter Zn isotopes has been associated with the presence of high- and low-affinity transport systems, respectively (Weiss et al. 2004; Caldelas and Weiss 2017). The type of transport system is dependent on the bioavailability of the metal, *e.g.* a high level of available Zn favours lighter isotopes uptake through low affinity transports, while a lower availability of the metal induces uptake of heavy isotopes through high affinity transporters (Tang et al. 2016). For Zn, it has been suggested that further fractionation from roots to higher parts of the plant can take place during the xylem loading process and subsequent transportation (Tang et al. 2016).

In the case of Ni, the physiological mechanisms regulating metal homeostasis are still largely unknown (Deng et al., 2014), but few studies posit that Ni sorption and translocation are regulated by low-affinity transport systems, and no high-affinity transport systems have been discovered hitherto in higher plants (Cataldo et al. 1978; Deng et al. 2014, 2019). Studying Ni isotopic fractionation and the homeostasis of the hyperaccumulator *Alyssum murale* grown in controlled hydroponic conditions, a preferential sorption of lighter isotopes from solution was observed ($\Delta^{60}Ni_{plant\text{-}solution}$ = -0.9 to -0.63 ‰) (Deng et al. 2014). It is still unclear, however, how and at which stage Ni isotopic fractionation exactly takes place. Studying plants collected in the temperate ultramafic area of Albania, Estrade et al. (2015) reported an enrichment in heavier isotopes of Ni in the plants compared to the bulk soil, $\Delta^{60}Ni_{whole\ plant\text{-}soil}$ up to 0.40 ‰. Nevertheless, the Ni taken up by plants was lighter than the bioavailable Ni, extracted by diethylenetriaminepentaacetic acid (DTPA), and the difference $\Delta^{60}Ni_{available\text{-}rhizo\ soil}$ was up to 0.89 ‰. This result suggests that hyperaccumulating plants take up lighter isotopes from the heavier bioavailable Ni pool in soils. However, a recent study on hyperaccumulators in the tropical ultramafic region of Brazil, did

not report on any significant Ni isotopic fractionation neither during Ni uptake, nor during Ni translocation within the plants (Ratié et al. 2019). In our previous work, we have studied the remobilization of Ni by simulating the effect of leaf litter degradation of *A. murale* and *R.* cf. *bengalensis*. Obtained results showed that, in the case of *R.* cf. *bengalensis*, depending on the entity of the fractionation factor between roots and leaves, Ni recycling can result in a lighter isotope input into the surface soil (Zelano et al. 2018). Nickel hyperaccumulators, therefore, are responsible not only for "phyto-enrichment" of Ni concentration in surface soil, but they can also influence its isotopic composition. However, a clear mechanistic understanding of the observed Ni isotopic signatures in the soil-plant system and the links with the processes responsible for Ni isotopic fractionation have not been attained thus far. Only few publications have attempted to decipher the metal dynamics in the soil-root-shoot continuum by combining stable isotope tool and speciation data (Aucour et al. 2015, 2017). In this work, we developed an analytical strategy to follow Ni transfer from soil to plant shoots, considering the soil characteristics and the vertical distribution of Ni in the different horizons. Furthermore, in order to better understand the dynamics of Ni during the growth of a woody tropical hyperaccumulator tree, we investigated two differently aged plants. As such, this study focuses on two related soil-plant systems of *R.* cf. *bengalensis* naturally occurring on ultramafic soils, in the tropical rainforest of Kinabalu Park (Sabah, Borneo Island, Malaysia) (van der Ent and Mulligan 2015; van der Ent et al. 2015, 2018c; 2020). Two differently sized/aged plants were sampled on two distinct soils having two different stages of pedogenesis. On the basis of Ni concentrations, Ni speciation and δ^{60}Ni in soils and plants, first results on the Ni dynamics in the soil-plant system are provided and interpreted**.**

Materials and methods

All reagents were prepared using ultrapure water (18.2 MΩ cm). Nitric and hydrochloric acids were of supra-pure grade. Standard solutions were supplied by TechLab (1000 µg mL^{-1}, in a 2–5% HNO_3).

Plant material and soil collection

Two individuals of *R.* cf. *bengalensis* were sampled in the native equatorial rainforest of Sabah, (Borneo Island, Malaysia). The plants naturally developed on soils derived from serpentinized and non-serpentinized ultramafic bedrock (for a detailed overview of the characteristics of the local soils, see van der Ent et al. 2018a; 2019b). The first specimen, R_{150}, measuring 150 cm high, was collected on a deeply weathered Ferralsol near Serinsim (Nkrumah et al. 2018). The other individual, R_{600}, is a tree of approximatively 6 m tall, and was collected near

120 Lompoyou Hill, on an eroded hypermagnesian Cambisol on strongly serpentinized bedrock (Nkrumah et al.
121 2018; van der Ent et al. 2018a). According to a recent study (Nkrumah et al. 2019a,b), the R_{150} and R_{600} trees are
122 estimated to be less than 1 year and about 3 years old, respectively. Although such trees are common in this area
123 of the world, trees of different age were only found in distinct areas during our one-week campaign. This study
124 is, therefore, focused on two trees of different age, respectively grown on a Ferralsol and on a Cambisol.
125
126 The R_{150} plant was harvested in its entirety and was subsequently divided into roots, trunk (later subdivided in
127 bark and wood samples) and leaves. For R_{600}, multiple leaf and bark samples were collected along the entire
128 height of the plant, from 1–6 m. Two phloem tissue samples were extracted by stripping the inner bark from the
129 wood core at 5 cm under and 5 m above soil level. In the young tree, the phloem tissue is thin and nearly
130 impossible to sample (van der Ent and Mulligan 2015), therefore samples were collected only for R_{600}. Two root
131 samples, considered to be surface roots, were also collected at about 5 cm and 15 cm under soil level. Deeper
132 root samples could not be collected.
133
134 The surface soils, between 0 cm and 15 cm depth, were collected at the base of R_{150} and R_{600} and referred to as
135 SR_{150} H1 (0–5 cm horizon), SR_{150} H2 (5–15 cm horizon), and SR_{600} H1 (0–5 cm horizon), SR_{600} H2 (5–10 cm
136 horizon) and SR_{600} H3 (10–15 cm horizon) respectively. About 500 g for each sample were collected. Several
137 rain forest species, including *R.* cf. *bengalensis*, are very shallow rooting and most of the nutrient cycling
138 happens in the top layer of the soil (Vitousek 1984; Vitousek and Sanford 1986), so only superficial soil horizons
139 were collected. Soils and plant samples were air-dried immediately after field collection, at temperature below
140 40°C. This preparation mode was selected due to the sampling conditions and the sampling location was not
141 compatible with the use of liquid nitrogen to preserve biological samples *in situ*. This mode of preparation is not
142 usually recommended for XAS measurements, and the drying step may have influenced the chemical speciation
143 of Ni, replacing water molecules by other ligands. The breaking of cell walls and membranes during the drying
144 could have induced the dissociation of Ni complexes with low stability. However, XAS results obtained on
145 plants show that the Ni speciation was not drastically modified by drying and the results are consistent with
146 published data (van der Ent et al. 2017).
147
148 Due to their apparent difference in particle size distribution, soils were sieved to compare similar size fractions.
149 Each soil sample was, then, subdivided in two equivalent parts; one was kept and referred to as 'bulk sample',

whereas the second part was sieved into four fractions, *i.e.* >1.5 mm; 1.5 mm – 250 µm; 250–50 µm and <50 µm.

Element concentration

All soil and plant samples were dried in a dehydrating oven at 110˚C overnight, and manually ground using an agate mortar. About 50–70 mg of ground plant material was weighed in Savilex® beakers and left overnight in 3–5 mL of concentrated (70%) HNO_3 at room temperature. Samples were, then, heated to 140˚C on a hot plate to complete the acid digestion. When necessary, a second digestion step was performed, using 3 mL of Aqua Regia and 1–2 ml of HF (32%) to allow for complete sample dissolution. Solutions were finally dried at 110˚C, recovered with 0.3 M $HNO_3$and measured with Inductively Coupled Plasma Mass Spectrometer (ICP-MS Quadrupole, X-Series Thermo Fisher Scientific).

Major and trace elements in soil samples were analysed by Service d'Analyse des Roches et des Minéraux (SARM), at Centre de Recherches Pétrographiques et Géochimiques, Nancy, France. The content of organic carbon in soils was measured using the EMIA-Analyser Carbon/Sulfur supplied by HORIBA, after decarbonation with HCl and filtration.

To estimate the available Ni concentration in soil samples, an aliquot of bulk soil was suspended in ultra-pure water for 24h, in triplicate, using 100 mg soil and 40 mL of milli-Q water. The final suspension was centrifuged for one hour at 52000 g and the resulting supernatant was filtered through 0.22 µm with cellulose syringe filters. Nickel concentration was measured in solution and, as an approximation, will be indicated hereafter as 'available Ni'. Reported results of available Ni concentration correspond to the average values of experimental triplicates. The bioavailable Ni pool in soils is operationally determined by chemical extraction using organic ligands, e.g. DTPA (Echevarria et al. 2006). By performing, however, a water extraction we exclude any potential isotopic fractionation arising from the Ni-ligand complex formation.

The cation exchange capacity (CEC) of the bulk soils was determined using cobalt hexammine. Briefly, 30 mL of 0.05 N hexammine cobalt(III) chloride were added to 1 g of dry soil, shaken for two hours at 30 ˚C and centrifuged at 52000 g. Supernatants were filtered through 0.22 µm and the residual concentration of hexammine analysed with UV spectrometry. This makes possible to determine the total CEC of the soil. Furthermore,

element concentrations (Na, Ca, K, Mg, Fe, Al, Si and Ni) in the supernatants were measured using a Thermo Fischer ICAP 6500 Inductively Coupled Plasma Optical Emission Spectrometer (ICP-OES).

Nickel isotope measurements

Prior to Ni isotopic measurement, a two-step chromatography separation was performed to remove sample matrix. The reported procedure is based on a previously developed protocol (Cameron et al. 2009; Gueguen et al. 2013) and modified as described by Estrade et al. (2015) and Deng et al. (2014). Briefly, soil and plant samples were digested, as described above, to determine, Ni content. Depending on the measured Ni concentration (verified after digestion using a Q-ICP-MS X series 2 Thermo-Scientific), a known volume of dissolved sample was evaporated to give a mass of Ni between 1 and 2 µg. After evaporation, the residue was dissolved again in 2 mL of 3 M HNO_3. In order to correct for any isotope composition variation potentially induced by the chemistry process, and for an instrumental mass bias, the technique of a double-spike addition was adopted. For that, a double-spike solution containing an equal amount of ^{61}Ni and ^{62}Ni isotopes was added to samples. The volume of double-spike solution to add was adapted for each sample to obtain a spike/sample ratio of 1.15. The mix was left equilibrating overnight, evaporated on a hot plate at 110˚C and dissolved in 1 mL of 6 M HCl. Solution was, then, passed on the first chromatographic column filled up with 2 ml of the anion-exchange resin AG®1-X8 and recovered. The resin, which is in chloride form, is able to retain Fe and Zn present in the sample matrix, while Ni is eluted with the solution. Additional 15 mL of 6 M HCl were passed through the column to recover all Ni. The final volume was successively evaporated on a hot plate at 110˚C and dissolved again in 1 mL HCl 1 M. The second chromatographic separation to complete the sample purification is based on the use of a Ni specific resin, supplied by Triskem Inc., France. The used resin is able to retain Ni through chelation with dimethylglyoxime at pH value 8–9. Before the second chromatographic separation, 0.2 mL of ammonium citrate ($(NH_4)_6C_6H_6O_7$) were added to the samples, the pH was adjusted at 8–9 with 100–150 µL of ammonia, and samples were left overnight for equilibration. Solution was loaded on the column and Ni retained by the resin was successively recovered by 4 mL of 3 M HNO_3 and put to evaporate on a hot plat at 110˚C. To eliminate any potential residue, acid digestion with aqua regia were performed, before recovery the sample with 0.3 M HNO_3 for measurement. Procedural blanks were prepared in each sample batch, resulting in 0.058–0.256 nmol of Ni content that has a maximum value of 1.5 % of the total Ni, and a corresponding negligible influence on reported isotopic values, within uncertainties.

The solutions were measured by Multi-Collector Inductively Coupled Plasma Mass Spectrometer (MC-ICP-MS, Neptune plus, Thermo Scientific) in medium resolution mode and using an Apex HF desolvation introduction system in a 0.3 M HNO_3 media. Ni masses (58, 60, 61, 62) were measured simultaneously as well as Cu isotopes and one Fe isotope at masses 63, 65 and 57 respectively. The ^{57}Fe intensity was monitored continuously to correct for any ^{58}Fe contribution to ^{58}Ni. The correction is effective only for a signal lower than 10 mV. When the signal was higher than 10 mV, samples were processed and eluted again through the first column. A standard bracketing method was used during sample measurements and $\delta^{60}Ni$ in samples were normalized to NIST-986. Sample $\delta^{60}Ni$ values were calculated as:

$$\delta^{60}\mathrm{Ni} = \left(\frac{^{60/58}\mathrm{Ni}_{\mathrm{sample}}}{^{60/58}\mathrm{Ni}_{\mathrm{NIST\ 986}}} - 1\right) \times 1000 \text{ in } (‰) \quad (1)$$

The analytical reproducibility was monitored by processing and measuring a Ni ICP-MS standard solution for each measurement session. Since no value exist for this solution, the standard subjected and not-subjected to the entire sample preparation procedure was measured and compare to itself, in order to control for isotopes composition modification during the process. The obtained average value was $\delta^{60}Ni = -0.11 \pm 0.05$ ‰ (2σ, n = 25). The reference material BHVO-2 was processed and measured ten times in different measurement sessions, obtaining $\delta^{60}Ni = 0.05 \pm 0.04$ ‰ (2σ), in agreement with published data (Gall et al. 2013; Gueguen et al. 2013; Estrade et al. 2015; Ratié et al. 2015). Estimated recovery from the measured intensities is always higher than 90%. However, recovery is not a crucial parameter as the double spike addition technique was used. In addition, in order to have a matrix match reference for plant samples, the Oak Leaves reference material V464 from the French National Institute for Agricultural Research (INRA) was also digested, purified and measured. The value obtained for this material is $\delta^{60}Ni = -0.02 \pm 0.05$‰ (2σ, N=6).

All samples were measured three times. The soil-water suspension samples to determine available Ni were prepared in triplicate. For those samples, the reported $\delta^{60}Ni$ values correspond to the average X of experimental triplicates x_m. The associated standard error (2σ) is calculated as:

$$\sigma = \frac{sd}{\sqrt{N}}, \quad (2)$$

where *sd* is the standard deviation of the sample mean, and N is the number of samples.

For bulk soil and plant material samples, no experimental triplicates are available and the reported 2σ represent the analytical error deriving from three measurements of the sample. The 2σ = 0.05 ‰ obtained for the Ni ICP-MS standard (digested and measured 25 times) was applied to all sample results presenting analytical 2σ < 0.05 ‰.

The Ni isotopic fractionation between two samples A and B, $\Delta^{60}Ni_{A\text{-}B}$, was calculated as the difference between the isotopic signatures measured in A and B, as reported below:

$$\Delta^{60}Ni_{A\text{-}B} = \delta^{60}Ni_A - \delta^{60}Ni^{2+}_B \quad (3)$$

The standard deviation σ associated to $\Delta^{60}Ni$ includes the error propagation and was calculated as:

$$y = a \pm b, \quad \sigma y = \sqrt{(\sigma a)^2 + (\sigma b)^2} \quad (4)$$

Soil mineralogical composition

The mineralogical composition of the samples was determined by X-ray diffraction (XRD, Bruker D8 Advance) with an X-ray tube producing Co Kα radiation (1.78886 Å) operated at 35 kV and 45 mA. The XRD patterns were obtained by scanning crushed powders of the sieved fractions and of the bulk soil, from 3° to 64° 2θ with a 0.035° 2θ step and with a 3s counting time per step. The diffracted signal was measured using a LynxEye detector with an energy discrimination window adjusted to minimize the high fluorescence background signal coming from Fe to improve the peak-to-background ratio.

Soil mineralogy was also investigated with electron microscopy, and transmission electron images were obtained with a Philips CM20 transmission electron microscope (TEM), operating at 200 kV, coupled to an Energy-Dispersive X-ray Spectrometer (EDXS). For TEM imaging and microanalysis, a few milligrams of sample were re-suspended in ethanol using ultrasonication (10 min) and a drop of suspension was evaporated on a carbon-coated copper grid. The EDX spectra were obtained in nanoprobe mode (20–30 nm) using a counting time of 40–70 seconds.

Chemical speciation of nickel (X-ray absorption spectroscopy)

X-ray absorption spectroscopy (XAS) experiments were performed at two beamlines, in fluorescence mode at the SAMBA beamline (SOLEIL synchrotron, France), and in transmission mode at the XAFS beamline (ELETTRA synchrotron, Italy). In both cases, Ni K-edge X-ray absorption spectra (both in the XANES and EXAFS regions) were recorded at low temperature (using a liquid He cryostat 25 K and liquid N_2 cryostat, 77 K respectively) with a Si(111) double crystal monochromator. A Ni foil was positioned after the sample and collected simultaneously to each spectrum in order to have perfect energy calibration; the first inflection point of metal Ni spectrum was calibrated at 8333 eV. Soil samples were scanned at SAMBA in fly scan mode from 8000 to 9500 at velocity of 5 eV/s, resulting in energy step of 0.5 eV, using an X-ray fluorescence detector (VORTEX, Hitachi). For each soil sample, between 22 and 35 spectra were recorded. Dried leaf samples were measured at the XAFS beamline in transmission detection mode, with three scans recorded in a step by step mode, with 5 eV steps for the first 200 eV, 0.2 eV for the XANES range and with a k-constant step of 0.03 ($Å^{-1}$) in the EXAFS range. In all cases, the samples were ground and pelletized before the XAS measurements. Reference spectra were obtained on the SAMBA and XAFS beamlines from previous sessions, under the same acquisition conditions. These standards included Ni aqueous solution with and without organic ligands, Ni incorporated into goethite, Ni sorbed onto phyllosilicate (charged and non-charged minerals), Ni sorbed onto calcite, Ni sorbed onto iron oxyhydroxide (goethite), and natural Ni containing minerals including chrysoprase, nimite, and Ni-bearing serpentine (clay mineral).

The XANES and EXAFS data were reduced using standard normalization procedures performed with the ATHENA and ARTEMIS programmes (Ravel and Newville 2005). The spectra were background subtracted, and normalized. A spline function was fit through the absorption envelope and subtracted from each spectrum. To transform data from energy space E (eV) to wave vector space k ($Å^{-1}$), E_0 edge energy was chosen in the higher part of the edge step, at 8343 eV. The resulting χ function was weighted by k^3 to avoid oscillations damping at high χ values. The EXAFS signals obtained from plant and soil samples were fitted as linear combinations of the standard EXAFS spectra collected on solutions and solid samples. The number of components was set to a maximum of three on the basis of TEM and XRD observations. The fitting parameters were then selected on the basis of quality indicators (χ^2, r-factor and reduced χ^2). Shell by shell fitting was also performed using theoretical scattering paths calculated from the unit cell structure of distinct Ni-bearing phases (Artemis code on the basis of FEFF6) (Ravel and Newville 2005; Rehr et al. 2010).

Results

Chemical and mineralogical composition of soils

The elemental concentrations were determined in the different horizons of soils associated with plants, SR_{150} and SR_{600}, for the bulk samples and for the size fractions i) >1.5 mm, ii) 250–50 µm, and iii) <50 µm, of both H1 horizons (Table SI 1). The major element contents are typical for soils developed on ultramafic bedrock (van der Ent et al. 2018a). The Fe content is relatively high, especially in SR_{150}, where it reaches up to 34 and 39.8 % (Fe_2O_3 %), while it ranges from 4.6 and 22.1 % in SR_{600}, with a clear increasing trend with depth in the latter case. The Si content is rather similar in the surface horizons of SR_{150} and SR_{600}, with up to 28.9 and 29.2 % (SiO_2 %) respectively. However, this content tends to increase with depth for SR_{600}, reaching up to 36.9 and 35.4 % in the H2 and H3 horizons respectively. The third major element discriminating the soils is Mg, which reaches up to 1.6% (MgO %) in SR_{150} and which ranges between 10.9 and 13.4 % in the SR_{600} soil horizons. Organic carbon is higher in RS_{600} (11.84% in H1) than in RS_{150} (7.44% in H1) and in both cases organic carbon decreases with depth. The trace elements are slightly higher in SR_{150} than in SR_{600}. In general, no marked changes within the soil profile can be observed for all trace elements measured. These results are consistent with previously published data of ultramafic rhizosphere soils, collected in the same area in Sabah, that constitute the habitat of *R.* cf. *bengalensis* (van der Ent et al. 2015, 2017; 2020).

Nickel concentrations (Table 1) are higher in SR_{150} than in SR_{600}, reaching 113 µmol g^{-1} and only 61 µmol g^{-1}, respectively. In both cases, Ni concentration remains rather constant in the different horizons, but decreases with soil size fraction (from fraction >1.5 mm to fraction <50 µm). Available Ni in bulk samples was estimated by measuring Ni concentration in the supernatant from soil-aqueous suspension. For SR_{150}H1 and –H2, the concentration of available Ni is about 0.35 µmol g^{-1}, while it is 0.40 µmol g^{-1} in SR_{600}H1 and decreases in SR_{600}H2 and SR_{600}H3 to 0.19 µmol g^{-1} and 0.09 µmol g^{-1}, respectively.

The highest cationic exchange capacity (CEC) in both bulk soil samples (Table SI 2) is observed in the H1 horizons (54.6 mEq per 100 g and 22.7 mEq per 100 g in SR_{600}H1 and SR_{150}H1, respectively). In both cases, CEC decreases with depth as a result of the decrease of organic matter. As a general trend, SR_{600} has a higher CEC than SR_{150} and the difference in CEC between the two soils, about 32 meq $100g^{-1}$, mainly derives from the higher concentration of exchangeable Mg that reaches 42.4 mEq per 100 g in SR_{600}H1, but only 5.8 mEq per

100 g in SR_{150}H1. Exchangeable Fe was under the detection limit in all of the samples. Exchangeable Ni is similar in both H1 horizons, but its relative contribution to total CEC is 6% in SR_{150} and is less than 1 % in SR_{600}. Moreover, it slightly increases in SR_{150}H2, while it decreases in SR_{600}H2-H3.

The mineralogy, as revealed by both XRD and TEM data, supports the discrimination of SR_{150} and SR_{600} soils (Fig.1 and Fig. SI 1–2). SR_{600} XRD patterns (in all horizons and size fractions) show the presence of phyllosilicate phases, commonly encountered in ultramafic soils. The clay minerals are represented by chlorite, talc and 7Å minerals (i.e. serpentine and kaolinite) and are associated with other silicates such as quartz, feldspars and amphiboles, as well as Fe-oxyhydroxide (goethite). The mineralogy of SR_{600} relates to the presence of the serpentinized bedrock beneath and to a less advanced weathering of this soil. The XRD patterns have intense diffraction peaks from amphibole and chlorite minerals (Fig. SI 2). For the second soil SR_{150}, quartz, talc and goethite diffraction lines dominate XRD patterns. Those patterns are all drastically different from those obtained for the SR_{600} samples, with a smaller number of crystalline phases (Fig. SI 1), and the presence of goethite is consistent with the higher Fe content in the SR_{150} soil samples. For both soils, XRD data do not reveal any variation in the different horizons and size fractions. The XRD analysis of the clay fraction of SR_{600} shows the predominance of chlorite minerals, and additional 7Å minerals (from the serpentine or kaolinite groups).

The XRD analysis is sensitive to crystalline phases only and soils are commonly constituted of poorly crystalline or amorphous phases. To enhance the mineralogical investigations, TEM images and combined spectra (EDX) were acquired on the fine fraction (<50 μm) of the topsoil horizons from SR_{150} and SR_{600} (Figure 1). The TEM micrographs for SR_{150} reveal mainly talc and goethite particles. Associated EDX spectra show that in SR_{150} Ni is mainly associated with Fe-oxyhydroxides, including goethite. In SR_{600}, different types of clay minerals are observed, as well as several poorly defined phases. For SR_{150}, goethite appears to be the predominant Fe-bearing phase, while for SR_{600}, TEM analyses reveal the presence of amorphous Fe-oxyhydroxides, frequently containing Ni (shown by EDX analysis). In the latter sample, Ni was detected in most of the investigated particles, ranging from 0.3 to 0.9% (atomic percentage, EDX data) including silicate particles.

The XAS spectra and extracted EXAFS oscillations were used to determine the solid speciation of Ni in the soils (Fig. 2). The comparison of bulk and fine fractions in the two soils show that the solid speciation of Ni was similar for both size fractions. XANES spectra from SR_{150} and SR_{600} appear very similar, mainly due to the fact

that Ni has the same oxidation state (2+) and octahedral coordination. Some differences, however, can be observed in the XANES region and on EXAFS oscillations that are consistent with mineralogy results (TEM-EDXS and XRD). Superimposition of XANES spectra reveals slight differences in the position of the main edge and of the first oscillation (Fig. SI.3). Differences were also noticed in the EXAFS oscillations and associated Fourier transforms (Fig.2). Fourier transform curves (imaginary and magnitude parts) show that the slight differences between these two spectra come from the nature and distribution of atoms in the 2nd and further coordination spheres (Fig.2). Shell by shell fitting shows that for both soil samples, six atoms of oxygen at 2.03-2.1 Å surround Ni atoms, and dominate the backscattering signal (Table 2).

Shell-by shell fitting (Table 2) also indicates the presence of Fe atoms at 3.07 and 3.54 Å in the case of SR_{150}, supporting the hypothesis that a fraction of Ni is adsorbed onto Fe oxyhydroxides, or is inserted in the crystal lattice of Fe oxyhydroxides. This conclusion is consistent with the higher concentration of Fe (*i.e.* goethite) in this sample SR_{150} (See table SI 1). For SR_{600}, FEFF fitting also shows the presence of low Z atoms at 3.26 Å, supporting the hypothesis that a part of Ni is incorporated in the silicate structure. This result is also correlated with the high proportion of phyllosilicates in sample SR_{600} (XRD and TEM data). Linear combination fitting (Table 2) reveals matches with reference spectra in the samples SR_{600} and SR_{150}: Ni sorbed onto smectite (59 % and 50% for SR_{600} and SR_{150} respectively), Ni sorbed onto goethite (16% and 50% for SR_{600} and SR_{150} respectively, and Ni in serpentine (26% for SR_{600}) (Fig. 2).

Element concentrations and Ni chemical speciation in plant samples

Multi-elemental analyses were performed on different plant material of R_{150} and R_{600} which conform with concentrations ranges previously reported for *R.* cf. *bengalensis* (van der Ent et al. 2017; 2020). Results and detailed discussion are provided in Supplementary Information Table SI 3–4 and associated notes.

The R_{150} specimen was entirely collected and the mass of plant material was weighed. The whole dry plant weight was 91.96 g. The plant was then divided in leaf, root, bark and wood samples and, except for leaves, the quantification of their relative mass was difficult to achieve. However, an estimation of the relative mass of bark and wood was made, and on the basis of the corresponding Ni concentration, the total Ni content has been calculated to be 8018 µmol. The weighted average concentration in the whole plant was 87.20 ± 70.65 µmol of Ni per g of plant. The weighted standard deviation has been calculated as reported in equation 5:

$$sd_w = \sqrt{\frac{\sum_{i=1}^{N} wi(xi-xm)^2}{\frac{(N-1)\sum_{i=1}^{N} wi}{N}}}, \quad (5)$$

where *wi* is the weight for the *ith* observation, *N* is the number of non-zero weights, and *xw* is the weighted mean of the observations.

In line with data previously published for *R.* cf. *bengalensis* (van der Ent et al. 2017; 2020), Ni concentrations leaves are high, between 134 µmol g^{-1} and 221 µmol g^{-1} in R_{150} and, with the exception of leaves at 80 cm height, Ni slightly decreases from the bottom to the top of the plant (Table 4). In contrast, no clear trend can be observed in the bark samples where Ni concentrations range between 43 µmol g^{-1} and 98 µmol g^{-1}, decreasing from 20 cm to 60 cm and increasing again from 60 cm to 90 cm. Nickel concentrations in the wood samples have an increasing trend from the bottom to the top, from 6.68 µmol g^{-1} to 70 µmol g^{-1}. A different trend is observed in R_{600}, where Ni concentrations, both in leaf and bark samples, clearly decreases as a function of plant height: from 522 µmol g^{-1} in older leaves at 2 m, to 156 µmol g^{-1} in younger leaves at 6 m, and Ni concentrations in bark at the same height decreases from 133 µmol g^{-1} to 53 µmol g^{-1}. Two root samples per plant were collected at about 5 cm and 15 cm under the soil surface and Ni concentrations have similar range, 154 µmol g^{-1} and 81.7 µmol g^{-1} in R_{150}, and 63.2 µmol g^{-1} and 111 µmol g^{-1} in R_{600}.

Nickel chemical speciation in *R.* cf. *bengalensis* leaves was investigated (Fig. 3, Table 3) and the XAS spectra are rather similar evidencing that Ni speciation is predominated by Ni complexed with low molecular weight carboxylic acids (malate and citrate). These results are consistent with those previously reported (van der Ent et al. 2017), and suggest that Ni chemical speciation was not drastically changed by the drying step. XAS spectra could not reveal any differences of chemical speciation of Ni in the investigated *R.* cf. *bengalensis* specimen. Linear combination fitting suggests the contribution of hydrated cations $Ni^{2+}(H_2O)_6$ at 33% and 31% for R_{600} and R_{150} respectively, the presence of Ni-malate complexes at 41% and 42% for R_{600} and R_{150} respectively, and Ni-citrate complexes at 26% and 27 % for R_{600} and R_{150} respectively.

The chemical speciation of Ni in *R.* cf. *bengalensis* leaves supports the idea that Ni is not strongly chelated by specific organic molecules and is not considered as a contaminant or as xenobiotic by the plants. The apparent weakly bound state of Ni makes it readily mobile, and Ni might be not permanently stored within the leaves.

XAS data do not reveal any differences between the R_{600} and R_{150} leaves, suggesting that Ni remains relatively mobile, whatever the age of the tree.

Nickel isotopic composition in soils and plants

The $\delta^{60}Ni$ values in bulk soils ($\delta^{60}Ni_{bulk}$) and in the available fraction ($\delta^{60}Ni_{available}$) are shown in Table 1. The bulk soil horizons of SR_{150} and SR_{600} have slightly different Ni isotopic signatures, $\delta^{60}Ni_{bulk\_RS150\_H1}$ = -0.17 ± 0.05 ‰, $\delta^{60}Ni_{bulk\_SR150\_H2}$ = -0.16 ± 0.05 ‰, and $\delta^{60}Ni_{bulk\_RS600\_H1}$ = -0.01 ± 0.05 ‰, $\delta^{60}Ni_{bulk\_RS600\_H2}$ = 0.01 ± 0.06 ‰, respectively. In both cases, $\delta^{60}Ni$ does change neither with depth, nor in the <50 µm fractions of H1 compare to the bulk. The SR_{150} H1 available Ni ($\delta^{60}Ni_{available\_RS150\_H1}$) is slightly enriched in lighter Ni isotopes in comparison with the corresponding bulk soil SR_{150} ($\delta^{60}Ni_{available\_RS150\_H1}$ = -0.32 ± 0.09 ‰), obtaining $\Delta^{60}Ni_{bulk–available\_RS150\_H1}$= 0.15 ± 0.10 ‰. However, this result is not observed for the lower horizon SR_{150}H2, where available Ni is similar to the bulk soil, $\delta^{60}Ni_{available\_RS150\_H2}$= -0.14± 0.05 ‰, and $\Delta^{60}Ni_{bulk\text{-}available\_RS150\_H2}$= -0.02 ± 0.07 ‰. On the contrary, SR_{600} available Ni has an enrichment in heavier Ni isotopes, increasing with soil depth, $\delta^{60}Ni_{available\_RS600\_H1}$ = 0.32 ± 0.05 ‰, $\delta^{60}Ni_{available\_RS600\_H2}$ = 0.52 ± 0.05 ‰ and $\delta^{60}Ni_{available\_RS600\_H3}$ = 0.62 ± 0.05 ‰. The isotopic difference with the corresponding bulk soils were calculated as $\Delta^{60}Ni_{bulk\text{-}available\_RS600\_H1}$= -0.33 ± 0.06 ‰ and $\Delta^{60}Ni_{bulk\text{-}available\_RS600\_H2}$= -0.51 ± 0.07 ‰.

The Ni isotopic composition of the two *R.* cf. *bengalensis* specimens R_{150} and R_{600} are reported on Table 4. The root samples from R_{150} plant at -5 cm and -15 cm under the surface level has $\delta^{60}Ni_{roots}$ = -0.35± 0.05 ‰ and $\delta^{60}Ni_{roots}$ = -0.42 ± 0.05 ‰, respectively. Similarly, the surface roots of R_{600} plant, both collected at -5 and -15 cm under surface level, has negative values, -0.58± 0.05‰ and -0.59 ± 0.06 ‰ respectively (Table 4).

In the aerial parts, $\delta^{60}Ni$ in leaves of R_{150} is between -0.66 and -0.89 ‰, clearly showing a preferential translocation of light Ni isotopes from the roots to the leaves (Tables 4 and 5) and, among the leaves, from the bottom to the top, with the presence of lighter Ni isotopes in the younger apical leaves. Moreover, it can be seen from Fig.4 that leaves, which constitute the Ni-enriched parts of the plants (table 4), have $\delta^{60}Ni$ values lighter than the ligneous material, *i.e.* wood and bark. The wood and bark samples have relatively wide-ranging values. However, with the exception of the wood sample at 100 cm, a preferential concentration of heavier Ni isotopes can be observed from the bottom to the top of the plant. The $\delta^{60}Ni$ value of the whole plant R_{150} was estimated by calculating the weighted mean of the $\delta^{60}Ni$ in the different parts of the plant,

resulting in a value of -0.65 ± 0.23 ‰. The weighted standard deviation was calculated as reported in eq 5.

The $\delta^{60}Ni$ values in R_{600} leaves range between -0.19 ‰ and -0.33 ‰, but no systematic variation is observed between the basal and apical leaves, collected from 2 to 6 m. Moreover, bark samples also have variable $\delta^{60}Ni$ values, from -0.29 ‰ to 0.15 ‰, in some cases heavier and in others lighter than the leaves collected at the same height, without any clear trend. The phloem tissue sample collected from beneath the bark at – 5 cm has a similar isotopic composition than root collected at the same level, $\delta^{60}Ni_{phloem}$ = -0.60 ± 0.08 ‰. The phloem tissue at 5 m high has, on the contrary, a heavier Ni isotopic composition ($\delta^{60}Ni_{phloem}$ = -0.10 ± 0.06 ‰), than leaf and bark at the same height, $\delta^{60}Ni_{leaf}$ = -0.30 ± 0.05 ‰ and $\delta^{60}Ni_{bark}$ = -0.13 ± 0.09 ‰, respectively. However, the anomalously low Ni concentration in this sample collected at 5 m suggests a collection error and, therefore, it will not be included in the further discussion.

Discussion

Nickel isotopic composition in soil

The studied soil samples have two distinct stages of pedogenesis, which are reflected not only by the overall element concentrations and associated mineralogy, but also by their Ni isotopic composition. Weathering processes are expected to influence $\delta^{60}Ni$ by depleting the heavier fraction of Ni in soil (Ratié et al. 2015). This hypothesis is consistent with the lighter Ni isotopic signature of SR_{150} bulk ($\delta^{60}Ni$ = -0.17 ± 0.05) compare to SR_{600} bulk ($\delta^{60}Ni$ = -0.01 ± 0.05). The SR_{150} is a Ferralsol, collected near Serinsim region, and can be considered to have reached steady state equilibrium, as in Ferralsols all the alterable minerals have been weathered and secondary minerals carry most of the Ni in this soil. This assumption is supported by the soil mineralogy, characterized by a quasi-absence of phyllosilicates, and by the Ni solid speciation, showing that Ni is mainly bound to poorly crystalline Fe oxyhydroxides. Moreover, no difference is detected between the two first SR_{150} soil horizons H1 and H2, which have similar total and available Ni concentrations, and similar isotopic composition. The available Ni from H1 is slightly enriched in light isotopes ($\Delta^{60}Ni_{bulk\text{-}available}$= 0.15±0.10 ‰), while no fractionation is observed for H2 ($\Delta^{60}Ni_{bulk\text{-}available}$ = -0.03 ±0.07 ‰). Such a stable isotopic composition of $\Delta^{60}Ni_{bulk\text{-}available} \sim 0$, can be the result of the loss of the heavier water soluble Ni from the soil, due to full weathering of the primary minerals, achieved after thousands of years. In contrast, the soil SR_{600} is a partially weathered hypermagnesian Cambisol and the soil isotopic composition suggests the contribution of other processes than in SR_{150}. Primary and secondary phyllosilicates, in which Ni is often present

in structural positions and/or adsorbed onto the surface forming outer-sphere complexes (Chardot et al. 2007; Raous et al. 2013; Bani et al. 2014), are the main crystalline phases. To a lesser extent, Ni is also associated to amorphous Fe oxides (Fig.1). Both total Ni concentration and δ^{60}Ni values in bulk soils remain constant in the three horizons of SR_{600}, i.e. H1, H2 and H3. However, from H1 to H3, available Ni concentration decreases with depth and has a clear enrichment of heavy isotopes, with δ^{60}Ni values increasing from 0.32 ‰ to 0.62 ‰ from H1 to H3, respectively. These values are directly correlated with a decreasing of exchangeable Ni (see CEC values in Table SI 2), a decreasing of organic C, and an increasing of Fe content. Performing water extraction provides an estimation of the available Ni mainly involved in weak bonds with mineral surface groups or organic matter. Such a contribution to the available pool of Ni in surface horizon of ultramafic soils has already been noted (Zelano et al. 2015). The contribution of organic matter (OM) to available Ni is, therefore, likely more important in H1 and H2 than in H3, and it can be hypothesized that the increasing positive values of $\delta^{60}Ni_{available}$ in H2 and H3, are due to a lower proportion of weakly bound Ni in those horizons compared to SR_{600} H1. In the light of the results, it can be assumed that the lighter pool of available Ni in SR_{600}H1 is the result of combined processes, such as the prolonged Ni uptake by plant and the leaf litter degradation, during which Ni is released to surface soil, *in primis* to H1. Reported results have shown that Ni isotopic composition of the whole plant R_{150} is lighter than the available Ni in soil (Table 5), suggesting that *R.* cf. *bengalensis* takes up lighter Ni isotopes. This hypothesis can be reasonably extrapolated to the case of R_{600}, for which the calculation of a mass balance was not possible, but in which all plant material have an isotopic signature lighter than the available Ni in soil. In a previous study it has been shown that during leaf litter degradation process, about the 80 % of Ni released has the same δ^{60}Ni value of the original leaves, and that after a few days, a release of light isotopes occurs (Zelano et al. 2018). Therefore, the enrichment of lighter isotopes in the whole plant likely produces a release of lighter Ni isotopes during leaf litter degradation to topsoil, H1, compared to the deeper horizons, H2 and H3. However, this contribution might also vary depending on the potential isotopic fractionation between leaves and roots.

Nickel fractionation within plants

From the isotopic composition of both specimen R_{150} and R_{600}, it can be concluded that *R.* cf. *bengalensis* preferentially takes up the lighter Ni isotopes from the available Ni fraction in soil through absorption by root cells, as reported in Table 5. This result is consistent with previously published data for Ni hyperaccumulators grown in hydroponics, where it was also shown that the entity of the fractionation was due to a competition effect, induced by the concomitant presence of other metals, *e.g.* Zn (Deng et al. 2014). In the case of Zn

505 accumulation in wheat, a non-hyperaccumulating plant, it has been reported that the variation of Zn supply can
506 be a source of different trends of Zn isotopic fractionation in the soil-plant system. The lower availability of Zn
507 could enhance the release of organic ligands, such as phytosiderophores by the plant (Arnold et al. 2010), and
508 thus the Zn uptake from soil, with subsequent enrichment of the plant in heavy isotopes (Wiggenhauser et al.
509 2018). However, hyperaccumulators often have more specific processes of uptake and translocation of metals
510 than non-accumulating plants. For example, the Zn hyperaccumulator *N. caerulescens* has the ability to use both
511 high- and low-affinity transport systems depending on Zn availability, and this behaviour probably induces
512 different trends of Zn isotopic fractionation in the plants (Deng et al. 2014). In our case, the investigated *R.* cf.
513 *bengalensis* grew on ultramafic soils, and neither the scarcity of Ni nor the competition effect with other metals
514 can be considered as relevant factors determining Ni isotopic fractionation in the soil-plant system. In
515 hyperaccumulating plants, it has been assumed that Ni is taken up through a symplastic pathway, and that Ni
516 isotopic composition in whole plant derives from the uptake mechanisms of root cell membrane (Deng et al.
517 2014), promoting the uptake of lighter isotopes. Different pathways of fractionation within the plant parts can,
518 then, take place, but they are far from being fully understood. It has been recently reported that in wheat plants,
519 important Zn isotopic fractionation within plant parts can be attributed to the absorption of heavy isotopes to cell
520 walls in the apoplastic space (Wiggenhauser et al. 2018). However, through experiments based on the use of
521 radioactive ^{63}Ni, it was reported that Ni is transferred from roots to shoots via xylem, and also that its mobility is
522 greater than that of Zn, Mn, Co and Cd (Page and Feller 2005). These observations suggest that in
523 hyperaccumulators, Ni undergoes a very efficient translocation process that might not be the only source of
524 isotopic fractionation, or at most, it is responsible for the smaller isotopic fractionation observed for Ni compared
525 to *e.g.* Zn (Deng et al. 2014; Wiggenhauser et al. 2018) and Cd (Wiggenhauser et al. 2016). Whereas some
526 publications report demonstrations or assumptions about the translocation mechanisms of Ni (Kerkeb and
527 Krämer 2003; Alves et al. 2011), nothing is known about this mechanism for *R.* cf. *bengalensis.* In this study,
528 reported XAFS spectra on *R.* cf. *bengalensis* (Fig.3, Table 3) show that Ni in leaves is unequivocally present as a
529 complex with low molecular weight carboxylic acids (*i.e.* malate and citrate), confirming results reported by van
530 der Ent et al. (2017).
531
532 In the case of Zn and Cd, the isotopic fractionation in wheat shoots has been attributed to their different affinity
533 for functional groups of organic ligands (Wiggenhauser et al. 2018), or different chemical speciation. The
534 hypothesis about the possible influence of complexation with organic ligands on Ni isotopic fractionation was

previously investigated (Zelano et al. 2018). However, a rather low potential of fractionation induced by complexation reaction between Ni and citric acid, oxalic acid and purified humic substances was reported with a maximum value of $\Delta^{60}Ni_{bond\text{-}free} < 0.2$ ‰. Such a small fractionation can be excluded as a source of $\Delta^{60}Ni$ within plant material, discarding the hypothesis raised up for Zn fractionation in wheat shoots. The observed $\Delta^{60}Ni$ values within the two investigated specimen of *R.* cf. *bengalensis* cannot be fully explained by a complexation reaction or by different affinity towards organic molecules.

Despite only two specimens have been investigated in this work, one possible interpretation for the observed $\Delta^{60}Ni$ might come from the different age of the two *R.* cf. *bengalensis* plants. Even though they grew on different soils, both plants take up lighter Ni isotopes and the reported results suggest a correlation between the plant age and the observed $\Delta^{60}Ni$ values. Both specimens have the highest concentration of Ni in leaves, confirming that Ni is never stored in roots, but it is rapidly transferred to them, as it expected for Ni hyperaccumulators that do not require defence mechanisms against high Ni concentration in soil. In the early stage of growth of the plant (R_{150}), 80 % of the total amount of Ni is mobilized and more than 70 % is concentrated in leaves. This transfer produces a remarkable isotopic fractionation between leaves and roots, from which a preferentially translocation of lighter isotopes, $\Delta^{60}Ni_{root\text{-}leaf}$ up to 0.51 ± 0.07 ‰, can be observed (Table 5). At the same time, an enrichment of heavier isotopes in the ligneous parts of the plant is present. As the total amount of Ni in leaves is definitively higher than in wood and bark, these results strongly suggest that lighter isotopes are transferred first, going from roots to leaves. Data reported in Fig. 4 suggest, moreover, that the fractionation is correlated to the rate of Ni translocation (lighter isotopes move faster) as an important fractionation is also observed as a function of height, between younger (apical) and older (basal) parts of the plant. This implies that as soon as new leaves appear, Ni is mobilized through leaves, and lighter isotopes arrive first. This trend is no longer observed in the older specimen (R_{600}), where the isotopic fractionation between basal and apical leaves is not evident anymore. This result is surprising as Ni concentration still shows a clear trend between the apical and basal leaves, higher in basal, and lower in apical ones. Moreover, the isotopic fractionation between leaves and other plant material is less pronounced in the older specimen than in the younger plant (see Fig.4). This observation suggests that the fractionation observed in R_{150} is not necessarily attributable to different transport or retention mechanisms, as it is hypothesized for other metals, *e.g.* Cd (Wiggenhauser et al. 2016). If the fractionation were due to transport or retention mechanisms, it would be accentuated in the older plant, but the opposite result is observed. In addition,

564 in R_{600}, all plant material has lighter isotopes than soil available Ni, but all aerial parts (leaves, bark, wood) are
565 enriched in heavier isotopes compared to roots.
566
567 Taken together, the available data suggest that during the first period of growth, when the plant starts to take up
568 Ni, the transfer of light isotopes from roots to leaves can be due to kinetic effects. Once the amount of Ni
569 accumulated in the plant has increased (see Ni concentration in R_{600}, Table 4), the Ni already present in the plant
570 circulates through the phloem tissue into all plant parts. Successive loading and unloading cycles would have,
571 therefore, the effect to homogenize the isotopic fractionation among leaves, and between leaves and the other
572 plant components, erasing the difference between new and old leaves. In old specimens, the consequent
573 increasing number of cycles that Ni makes within the plant through the circulation of phloem sap from top to
574 bottom, and inversely, would reduce the isotopic fractionation. The observed data in R_{600} are probably the results
575 of several additive processes and support the idea that in the hyperaccumulator *R.* cf. *bengalensis*, Ni is involved
576 in plant homeostasis as any other cation. However, to confirm this hypothesis, supplementary data should be
577 collected on a wider population of trees of *R.* cf. *bengalensis,* collected in their natural habitat and at different
578 stage of growth.

579 ## Conclusions

580 This study aimed to unravel the biogeochemical processes resulting in Ni isotopic fractionation in two different
581 soil-plant systems associated with the Ni hyperaccumulator plant *R.* cf. *bengalensis.* The investigated soils have
582 distinct stages of pedogenesis, which are both highlighted by the mineralogical composition and the isotopic
583 signature of the available pool of Ni. The Ferralsol SR_{150} reflects a stable system, which has reached a steady-
584 state equilibrium, subsequent to the complete weathering of primary minerals and for which Ni is mainly
585 associated to poorly crystalline Fe-oxyhydroxides. The isotopic signature has no variation, neither in soil bulk
586 surface horizons, nor in the available pool of Ni. In the partially weathered hypermagnesian Cambisol SR_{600}, Ni
587 is associated not only to Fe-oxyhydroxides, but also to the identified phyllosilicates, and even though the Ni
588 isotopic composition of bulk soils does not vary, an enrichment in heavy isotopes is observed with depth for the
589 Ni available fraction. In both soil systems, the two investigated specimens of the hyperaccumulator *R.* cf.
590 *bengalensis* accumulate lighter Ni isotopes from the soil available Ni pool. The Ni isotopic composition in the
591 different parts of the plants were investigated and correlated to the plant height and age. Despite the limited
592 number of investigated samples, the study highlights the potential effect of plant age on Ni isotopic fractionation

593 in hyperaccumulator plants. A translocation of lighter isotopes of Ni from roots to leaves was observed in the
594 young plant, $\Delta^{60}Ni_{root\text{-}leaf}$ up to 0.51 ± 0.07 ‰, and isotopic fractionation was also unravelled between the apical
595 and basal leaves, $\Delta^{60}Ni_{basal\text{-}apical}$ up to 0.23 ± 0.07 ‰ (Table 5). However, this effect was not detected in the older
596 plant, where no isotopic fractionation was observed as a function of plant height, and where the Ni isotopic
597 fractionation seems to be mask by successive cycles of Ni circulation through the plant. These results suggest
598 that once Ni is taken up from the soil by roots, it is rapidly transferred to leaves, without being permanently
599 stored there. Instead, it has an active and continuous cycle within the plant through phloem-mediated
600 redistribution. Once the plant has accumulated a substantial quantity of Ni, the isotopic fractionation induced by
601 Ni translocation among aerial plant material is masked by an isotopic homogenization, and the observed isotopic
602 signature is the result of consecutive internal translocation cycles. However, it is still not clear why the roots of
603 the older specimen have a lighter isotopic signature than in aerial parts.
604
605 The acquired results suggest that it is inordinately difficult to discriminate between specific, individual processes
606 leading to Ni isotopic fractionation during Ni sorption and translocation within the plant, especially for
607 hyperaccumuating plants. The comparison of two plants with a different stage of growth seems to highlight the
608 role of plant`s age on Ni isotopic fractionation. However, to better constrain Ni homeostasis and the contribution
609 of *R.* cf. *bengalensis* to Ni isotopic signature in surface soil, more specimens should be investigated and
610 compared, both in the early and in the advanced stages of growth.
611
612 **Acknowledgements**
613 We thank Sabah Parks for granting permission to conduct research in Kinabalu Park, and the Sabah Biodiversity
614 Council for research permits. A. van der Ent is the recipient of a Discovery Early Career Researcher Award
615 (DE160100429) from the Australian Research Council. We thank Emile Benizri, Séverine Lopez, Celestino
616 Quintela-Sabaris and Sukaibin Sumail for their support during sampling campaign. We acknowledge IJL and
617 Mrs. Migot for access to TEM facilities. Parts of this research were carried out at SAMBA beamline at SOLEIL,
618 and at XAFS beamline from ELETTRA Synchrotron facility. We would like to thank Emiliano Fonda
619 (SOLEIL), Luca Olivi (ELETTRA) for assistance during the experiments. The research leading to this result has
620 been supported by the project CALIPSOplus under the Grant Agreement 730872 from the EU Framework
621 Programme for Research and Innovation HORIZON 2020. The authors would like to thank Agence Nationale de
622 la Recherche (ANR) project number ANR-14-CE04-0005-03 (AGROMINE) for funding. This is CRPG

623 contribution N°2567. The authors also would like to thank the two anonymous reviewers for their useful
624 suggestions that helped improving the quality of the manuscript.

625

626 **References**

627

628 Alves S, Nabais C, Simoes Goncalves M de L, Correia dos Santos MM (2011) Nickel speciation in the xylem
629 sap of the hyperaccumulator *Alyssum serpyllifolium* ssp. *lusitanicum* growing on serpentine soils of
630 northeast Portugal. J Plant Physiol 168:1715–1722. doi: 10.1016/j.jplph.2011.04.004
631 Arnold T, Kirk GJD, Wissuwa M, et al (2010) Evidence for the mechanisms of zinc uptake by rice using isotope
632 fractionation. Plant, Cell Environ 33:370–381. doi: 10.1111/j.1365-3040.2009.02085.x
633 Aucour A-M, Bedell J-P, Queyron M, et al (2015) Dynamics of Zn in an urban wetland soil–plant system:
634 Coupling isotopic and EXAFS approaches. Geochim Cosmochim Acta 160:55–69. doi:
635 10.1016/J.GCA.2015.03.040
636 Aucour AM, Bedell JP, Queyron M, et al (2017) Zn Speciation and Stable Isotope Fractionation in a
637 Contaminated Urban Wetland Soil-*Typha latifolia* System. Environ Sci Technol 51:8350–8358. doi:
638 10.1021/acs.est.6b02734
639 Baker AJM Metal Tolerance. New Phytol. 106:93–111
640 Baker AJM (1981) Accumulators and excluders □strategies in the response of plants to heavy metals. J Plant
641 Nutr 3:643–654. doi: 10.1080/01904168109362867
642 Baker AJM, Brooks RR (1988) Botanical Exploration for Minerals in the Humid Tropics. J Biogeogr 15:221.
643 doi: 10.2307/2845062
644 Bani A, Echevarria G, Montargès-Pelletier E, et al (2014) Pedogenesis and nickel biogeochemistry in a typical
645 Albanian ultramafic toposequence. Environ Monit Assess 186:4431–4442. doi: 10.1007/s10661-014-3709-
646 6
647 Becquer T, Quantin C, Rotte-Capet S, et al (2006) Sources of trace metals in Ferralsols in New Caledonia. Eur J
648 Soil Sci 57:200–213. doi: 10.1111/j.1365-2389.2005.00730.x
649 Bonifacio E, Zanini E, Boero V, Franchini-Angela M (1997) Pedogenesis in a soil catena on serpentinite in
650 north-western Italy. Geoderma 75:33–51. doi: 10.1016/S0016-7061(96)00076-6
651 Boyd RS, Martens SN (1998) The significance of metal hyperaccumulation for biotic interactions.
652 Chemoecology 8:1–7. doi: 10.1007/s000490050002
653 Caldelas C, Weiss DJ (2017) Zinc Homeostasis and isotopic fractionation in plants: a review. Plant Soil 411:17–
654 46. doi: 10.1007/s11104-016-3146-0
655 Cameron V, Vance D, Archer C, House CH (2009) A biomarker based on the stable isotopes of nickel. Proc Natl
656 Acad Sci U S A 106:10944–8. doi: 10.1073/pnas.0900726106
657 Cataldo DA, Garland TR, Wildung RE (1978) Nickel in Plants: I. Uptake Kinetics Using Intact Soybean
658 Seedlings. PLANT Physiol 62:563–565. doi: 10.1104/pp.62.4.563
659 Chardot V, Echevarria G, Gury M, et al (2007) Nickel bioavailability in an ultramafic toposequence in the
660 Vosges Mountains (France). Plant Soil 293:7–21. doi: 10.1007/s11104-007-9261-1
661 Deng T-H-B, Cloquet C, Tang Y-T, et al (2014) Nickel and Zinc Isotope Fractionation in Hyperaccumulating

662 and Nonaccumulating Plants. Environ Sci Technol 48:11926–11933. doi: 10.1021/es5020955
663 Deng T-H-B, Tang Y-T, Sterckeman T, et al (2019) Effects of the interactions between nickel and other trace
664 metals on their accumulation in the hyperaccumulator *Noccaea caerulescens*. Environ Exp Bot 158:73–79.
665 doi: 10.1016/j.envexpbot.2018.11.015
666 Deng T-H-B, van der Ent A, Tang Y-T, et al Nickel hyperaccumulation mechanisms: a review on the current
667 state of knowledge. doi: 10.1007/s11104-017-3539-8
668 Echevarria G, Massoura ST, Sterckeman T, et al (2006) Assessment and control of the bioavailability of nickel
669 in soils. Environ Toxicol Chem 25:643–651. doi: 10.1897/05-051r.1
670 Elliott T, Steele RCJ (2017) The Isotope Geochemistry of Ni. Rev Mineral Geochemistry 82:511–542. doi:
671 10.2138/rmg.2017.82.12
672 Estrade N, Cloquet C, Echevarria G, et al (2015) Weathering and vegetation controls on nickel isotope
673 fractionation in surface ultramafic environments (Albania). Earth Planet Sci Lett 423:24–35. doi:
674 10.1016/j.epsl.2015.04.018
675 Gall L, Williams HM, Siebert C, et al (2013) Nickel isotopic compositions of ferromanganese crusts and the
676 constancy of deep ocean inputs and continental weathering effects over the Cenozoic
677 Gueguen B, Rouxel O, Ponzevera E, et al (2013) Nickel Isotope Variations in Terrestrial Silicate Rocks and
678 Geological Reference Materials Measured by MC-ICP-MS. Geostand Geoanalytical Res 37:297–317. doi:
679 10.1111/j.1751-908X.2013.00209.x
680 Gueguen B, Sorensen J V., Lalonde S V., et al (2018) Variable Ni isotope fractionation between Fe-
681 oxyhydroxides and implications for the use of Ni isotopes as geochemical tracers. Chem Geol. doi:
682 10.1016/j.chemgeo.2018.01.023
683 Guelke M, von Blanckenburg F (2007) Fractionation of Stable Iron Isotopes in Higher Plants. Environ Sci
684 Technol 41:1896–1901. doi: 10.1021/es062288j
685 Imseng M, Wiggenhauser M, Keller A, et al (2019) Towards an understanding of the Cd isotope fractionation
686 during transfer from the soil to the cereal grain. Environ Pollut 244:834–844. doi:
687 10.1016/j.envpol.2018.09.149
688 Imseng M, Wiggenhauser M, Keller A, et al (2018) Fate of Cd in Agricultural Soils: A Stable Isotope Approach
689 to Anthropogenic Impact, Soil Formation, and Soil-Plant Cycling. Environ Sci Technol 52:1919–1928.
690 doi: 10.1021/acs.est.7b05439
691 Jaffre T, Brooks RR, Lee J, Reeves RD (1976) *Sebertia acuminata*: A Hyperaccumulator of Nickel from New
692 Caledonia. Science (80-) 193:579–580. doi: 10.1126/science.193.4253.579
693 Jaffré T, Reeves RD, Baker AJM, et al (2018) The discovery of nickel hyperaccumulation in the New
694 Caledonian tree *Pycnandra acuminata* 40 years on: an introduction to a Virtual Issue. New Phytol
695 218:397–400. doi: 10.1111/nph.15105
696 Jouvin D, Weiss DJ, Mason TFM, et al (2012) Stable Isotopes of Cu and Zn in Higher Plants: Evidence for Cu
697 Reduction at the Root Surface and Two Conceptual Models for Isotopic Fractionation Processes. Environ
698 Sci Technol 46:2652–2660. doi: 10.1021/es202587m
699 Kerkeb L, Krämer U (2003) The Role of Free Histidine in Xylem Loading of Nickel in *Alyssum lesbiacum* and
700 *Brassica juncea* 1. Plant Physiol 131:716–724. doi: 10.1104/pp102.010686
701 Mesjasz-Przybylowicz J, Przybylowicz W, Barnabas A, van Der Ent A (2015) Extreme nickel

hyperaccumulation in the vascular tracts of the tree *Phyllanthus balgooyi* from Borneo. New Phytol 209:1513–1526. doi: 10.1111/nph.13712

Nkrumah PN, Echevarria G, Erkine PD, et al (2019a) Growth responses of two tropical nickel hyperaccumulator plant species to nutrient dosing. J Plant Nutr Soil Sc 182(5): 715–728.

Nkrumah PN, Echevarria G, Erskine PD, et al (2019b) Soil amendments affecting nickel uptake and growth performance of tropical 'metal crops' used for agromining. J Geochemical Explor 203:78–86. doi: 10.1016/j.gexplo.2019.03.009

Nkrumah PN, Echevarria G, Erskine PD, Chaney RL, Sumail S, van der Ent A (2019c) Effect of nickel concentration and soil pH on metal accumulation and growth in tropical agromining 'metal crops'. Plant Soil 443(1): 27–39.

Nkrumah PN, Tisserand R, Chaney RL, et al (2019d) The first tropical 'metal farm': Some perspectives from field and pot experiments. J Geochemical Explor 198:114–122. doi: 10.1016/J.GEXPLO.2018.12.003

Page V, Feller U (2005) Selective transport of zinc, manganese, nickel, cobalt and cadmium in the root system and transfer to the leaves in young wheat plants. Ann Bot 96:425–434. doi: 10.1093/aob/mci189

Raous S, Echevarria G, Sterckeman T, et al (2013) Potentially toxic metals in ultramafic mining materials: Identification of the main bearing and reactive phases. Geoderma 192:111–119. doi: 10.1016/j.geoderma.2012.08.017

Ratié G, Jouvin D, Garnier J, et al (2015) Nickel isotope fractionation during tropical weathering of ultramafic rocks. Chem Geol 402:68–76. doi: 10.1016/j.chemgeo.2015.02.039

Ratié G, Quantin C, Maia De Freitas A, et al (2019) The behavior of nickel isotopes at the biogeochemical interface between ultramafic soils and Ni accumulator species. J Geochemical Explor 196:182–191. doi: 10.1016/J.GEXPLO.2018.10.008

Ravel B, Newville M (2005) ATHENA, ARTEMIS, HEPHAESTUS: data analysis for X-ray absorption spectroscopy using IFEFFIT. J Synchrotron Radiat 12:537–541. doi: 10.1107/S0909049505012719

Reeves RD (2003) Tropical hyperaccumulators of metals and their potential for phytoextraction. Plant Soil 249:57–65. doi: 10.1023/A:1022572517197

Reeves RD, Baker AJM, Jaffré T, et al (2018a) A global database for plants that hyperaccumulate metal and metalloid trace elements. New Phytol 218:407–411. doi: 10.1111/nph.14907

Reeves RD, Baker AJM, Jaffré T, et al (2018b) A global database for plants that hyperaccumulate metal and metalloid trace elements. New Phytol 218:407–411. doi: 10.1111/nph.14907

Rehr JJ, Kas JJ, Vila FD, et al (2010) Parameter-free calculations of X-ray spectra with FEFF9. Phys Chem Chem Phys 12:5503–5513. doi: 10.1039/b926434e

Spivak-Birndorf LJ, Wang SJ, Bish DL, Wasylenki LE (2018) Nickel isotope fractionation during continental weathering. Chem Geol 476:316–326. doi: 10.1016/j.chemgeo.2017.11.028

Tang Y-T, Cloquet C, Deng T-H-B, et al (2016) Zinc Isotope Fractionation in the Hyperaccumulator *Noccaea caerulescens* and the Nonaccumulating Plant *Thlaspi arvense* at Low and High Zn Supply. Environ Sci Technol 50:8020–8027. doi: 10.1021/acs.est.6b00167

Tang Y-T, Cloquet C, Sterckeman T, et al (2012) Fractionation of Stable Zinc Isotopes in the Field-Grown Zinc Hyperaccumulator Noccaea caerulescens and the Zinc-Tolerant Plant Silene vulgaris. Environ Sci Technol 120827161207002. doi: 10.1021/es3015056

van der Ent A, Baker AJM, Reeves RD, et al (2013) Hyperaccumulators of metal and metalloid trace elements: Facts and fiction. Plant Soil 362:319–334. doi: 10.1007/s11104-012-1287-3

van der Ent A, Mulligan DM (2015) Multi-element Concentrations in Plant Parts and Fluids of Malaysian Nickel Hyperaccumulator Plants and some Economic and Ecological Considerations. J Chem Ecol 41:396–408. doi: 10.1007/s10886-015-0573-y

van der Ent A, Erskine PD, Sumail S (2015) Ecology of nickel hyperaccumulator plants from ultramafic soils in Sabah (Malaysia). Chemoecology 25:243–259. doi: 10.1007/s00049-015-0192-7

van der Ent A, Callahan DL, Noller BN, et al (2017) Nickel biopathways in tropical nickel hyperaccumulating trees from Sabah (Malaysia). Sci Rep 7:. doi: DOI: 10.1038/srep41861

van der Ent A, Cardace D, Tibbett M, Echevarria G (2018a) Ecological implications of pedogenesis and geochemistry of ultramafic soils in Kinabalu Park (Malaysia). Catena 160:154–169. doi: 10.1016/j.catena.2017.08.015

van der Ent A, Mulligan DR, Repin R, Erskine PD (2018b) Foliar elemental profiles in the ultramafic flora of Kinabalu Park (Sabah, Malaysia). Ecol Res 33:659–674. doi: 10.1007/s11284-018-1563-7

van der Ent A, Przybyłowicz WJ, de Jonge MD, et al (2018c) X-ray elemental mapping techniques for elucidating the ecophysiology of hyperaccumulator plants. New Phytol 218:432–452. doi: 10.1111/nph.14810

van der Ent A, Ocenar A, Tisserand R, Sugau JB, Erskine PD, Echevarria G (2019a) Herbarium X-ray Fluorescence Screening for nickel, cobalt and manganese hyperaccumulation in the flora of Sabah (Malaysia, Borneo Island). J Geochem Explor 202: 49–58.

van der Ent A, Nkrumah PN, Echevarria G, Tibbett M (2019b) Evaluating soil extraction methods for chemical characterization of ultramafic soils in Kinabalu Park (Malaysia). J Geochem Explor 196: 235–246.

van der Ent A, de Jonge MD, Mak R, Mesjasz-Przybylowicz J, Przybylowicz WJ, Barnabas AD, Hugh HH (2020) X-ray fluorescence elemental mapping of roots, stems and leaves of the nickel hyperaccumulators *Rinorea* cf. *bengalensis and Rinorea* cf. *javanica* (Violaceae) from Sabah (Malaysia), Borneo. Plant Soil. In Press. doi:10.1007/s11104-019-04386-2

Vitousek PM (1984) Litterfall, Nutrient Cycling, and Nutrient Limitation in Tropical Forests. Ecology 65:285–298. doi: 10.2307/1939481

Vitousek PM, Sanford RL (1986) Nutrient Cycling in Moist Tropical Forest. Annu Rev Ecol Syst 17:137–167. doi: 10.1146/annurev.es.17.110186.001033

Wang SJ, Wasylenki LE (2017) Experimental constraints on reconstruction of Archean seawater Ni isotopic composition from banded iron formations. Geochim Cosmochim Acta 206:137–150. doi: 10.1016/j.gca.2017.02.023

Wasylenki LE, Howe HD, Spivak-Birndorf LJ, Bish DL (2015) Ni isotope fractionation during sorption to ferrihydrite: Implications for Ni in banded iron formations. Chem Geol 400:56–64. doi: 10.1016/j.chemgeo.2015.02.007

Weiss DJ, Mason TFD, Zhao FJ, et al (2004) Isotopic discrimination of zinc in higher plants. New Phytol 165:703–710. doi: 10.1111/j.1469-8137.2004.01307.x

Whittaker RH (1954) The Ecology of Serpentine Soils. Ecology 35:258–288. doi: 10.2307/1931126

Wiggenhauser M, Bigalke M, Imseng M, et al (2018) Zinc isotope fractionation during grain filling of wheat and

782 a comparison of zinc and cadmium isotope ratios in identical soil–plant systems. New Phytol 219:195–
783 205. doi: 10.1111/nph.15146
784 Wiggenhauser M, Bigalke M, Imseng M, et al (2016) Cadmium Isotope Fractionation in Soil–Wheat Systems.
785 Environ Sci Technol 50:9223–9231. doi: 10.1021/acs.est.6b01568
786 Zelano I, Sivry Y, Quantin C, et al (2015) Study of Ni exchangeable pool speciation in ultramafic and mining
787 environments with isotopic exchange kinetic data and models. Appl Geochemistry 1–11. doi:
788 10.1016/j.apgeochem.2015.09.021
789 Zelano IO, Cloquet C, Fraysse F, et al (2018) The influence of organic complexation on Ni isotopic fractionation
790 and Ni recycling in the upper soil layers. Chem Geol 483:47–55. doi: 10.1016/J.CHEMGEO.2018.02.023

Table 1. Nickel concentration, µmol g^{-1}, and isotopic composition $\delta^{60}Ni$, in: i) bulk soil horizons collected at the bottom of *R.* cf. *bengalensis* R_{150} and R_{600}; reported results are the average of three measurements for each sample with the corresponding instrumental standard deviation σ. The standard deviation obtained for the Ni ICP- MS standard solution ($\delta^{60}Ni$ = -0.11 ± 0.05 ‰) was applied to all sample results presenting analytical error 2σ < 0.05 ‰. ii) Concentration and isotopic composition of Ni in solution after 24h of soil suspension in ultrapure water. Results are the average of triplicate samples and σ values were calculated as described in eq. 2, $\sigma = \frac{sd}{\sqrt{N}}$, where *sd* is the standard deviation of the sample mean, and N is the number of samples. The reference material BHVO-2 was processed and measured ten times, obtaining $\delta^{60}Ni$ = 0.05 ± 0.04 ‰ (2σ).

Sample	Bulk soil Ni				Available Ni					
SR_{150} horizons	[Ni], µmol g^{-1}	σ	$\delta^{60}Ni$	2σ	[Ni], µmol g^{-1}	σ	$\delta^{60}Ni$	2σ	$\Delta^{60}Ni_{bulk-available}$	2σ
H1 Bulk	95.3	0.44	-0.17	0.05	0.35	0.02	-0.32	0.01	0.15	0.10
H2 Bulk	113	0.93	-0.16	0.05	0.34	0.0.02	-0.14	0.01	-0.02	0.07
H1 >1.5mm	85.8	0.86	/		/				/	
H1 250 - 50µm	77.6	0.78	/							
H1 < 50µm	84.5	0.85	-0.17	0.05						
Sample	Bulk soil Ni				Available Ni					
SR_{600} horizons	[Ni], µmol g^{-1}	σ	$\delta^{60}Ni$	2σ	[Ni], µmol g^{-1}	σ	$\delta^{60}Ni$	2σ	$\Delta^{60}Ni_{bulk-available}$	2σ
H1 Bulk	61.0	0.56	-0.01	0.05	0.40	0.02	0.32	0.03	-0.33	0.06
H2 Bulk	58.7	0.32	0.01	0.06	0.19	0.05	0.52	0.03	-0.51	0.07
H3 Bulk	60.3	0.35	/		0.09	0.01	0.62	0.02	/	
H1 >1.5mm	56.2	0.56	/		/				/	
H1 250 - 50µm	50.8	0.51	/							
H1 < 50µm	41.8	0.55	0.05	0.05						

Table 2. XAS data on SR_{150} and SR_{600} bulk soils, H1 horizons. 1-Summary of the local structural parameters derived from EXAFS data analysis (shell by shell fitting). The Ni EXAFS data were Fourier transformed over the k range Δk and fitted over the ΔR range to four single scattering paths involving O, Fe or Si atoms. The amplitude reduction factor S_0^2 was fixed to 0.9 as well as the energy shift on the basis of reference spectra analysis. The number of atoms of the first coordination shell was fixed to 6, but the number of atoms of other coordination shells was released. The distance R and disorder Δ^2 were varied for all the coordination shells. 2- Linear combination fitting was obtained on the fitting range Δk using as a maximum three components: Ni sorbed onto a purified clay in position of exchangeable cation, Ni sorbed onto goethite and Ni as structural cation in serpentine mineral.

1-Structural parameters									
	Fitting range Δk(Å^{-1})	Fitting range ΔR (Å)	shell	Number of atoms	R(Å)	σ^2(Å^2)	ΔE (eV)	S_0^2	R factor
SR_{150}	2.2-10	1.1-4	Ni-O	6	2.030±0.01	0.00418±0.001	-5.79	0.90	0.00015
			Ni-Fe	1.3±0.5	3.066±0.01	0.00423±0.001			
			Ni-Fe	1.2±0.7	3.54 ±0.02	0.00618±0.0012			
			Ni-O	2.6±0.6	3.82 ±0.02	0.00411±0.001			
SR_{600}	2.5-10.4	1.1-4	Ni-O	6	2.058 ±0.01	0.00454±0.001	-4.12	0.90	0.000038
			Ni-Fe	0.7±0.6	3.118 ±0.01	0.0049±0.001			
			Ni-Si	1.6±0.6	3.261 ±0.02	0.0051 ±0.0015			
			Ni-O	3±0.6	3.92 ±0.02	0.0050±0.0009			
2-Linear combination fitting parameters									
	Fitting range Δk(Å^{-1})	Ni sorbed onto Clay	Ni-Goethite	Ni-Serpentine					R factor
SR_{150}	2-10	50.3+5	49.7±5						0.098
SR_{600}	2-10	59 ±4	16±2	26±3					0.054

Table 3. XAS data on *R. bengalensis* leaves - Linear combination fitting was obtained on the fitting range Δk using as a maximum three components from a library of reference spectra obtained from organic complexes of Ni as well as from Ni aqueous solution. Ni-malate, Ni-histidine and Ni-citrate solutions were prepared at pH 6 with a metal/ligand ratio of 7.

Linear combination fitting parameters						
	Fitting range Δk($Å^{-1}$)	Ni aqueous	Ni-malate	Ni-histidine	Ni-citrate	R factor
R_{150}	2-10.5	31±4	42±8		27±4	0.026
R_{600}	2-10.5	33±3	41±6		26±4	0.020

Table 4. Plant mass (g), Ni concentration (µmol g^{-1}) and isotopic composition (δ^{60}Ni) of *R. bengalensis* R_{150} and Ni concentration (µmol g^{-1}) and δ^{60}Ni values of R_{600} specimens are reported, in blue and green, respectively. All results are the average of three measurements for each sample and the relative standard deviations correspond to the instrumental error. When the 2σ associated to δ^{60}Ni values are < 0.05 ‰, the value of 2σ = 0.05 ‰ obtained for Oak Leaves reference material V464 (δ^{60}Ni = -0.02 ± 0.05 ‰, N=6) is used. The Ni concentration and the δ^{60}Ni of the whole plant have been calculated as the weighted average values. The corresponding 2σ values are calculated according to equation 5.

R_{150}	Height	Mass, g	[Ni], µmol g^{-1}	σ	δ^{60}Ni	2σ		**R_{600}**	Height	[Ni], µmol g^{-1}	σ	δ^{60}Ni	2σ
Leaf	50cm	6	171	1.10	-0.66	0.05		Leaf	2 m	522	7.84	-0.33	0.04
	60 cm	7.6	156	0.62	-0.75	0.05			3 m	349	5.50	-0.19	0.05
	80 cm	4.7	221	1.60	-0.78	0.05			4 m	309	5.94	-0.20	0.04
	110 cm	8.5	134	2.40	-0.82	0.05			5 m	220	6.85	-0.30	0.02
	150cm	9.6	138	2.72	-0.89	0.05			6 m	156	1.17	-0.25	0.08
Bark								Bark	- 5 cm	9.56	0.04	0.12	0.05
	20 cm	0.5	68.7	0.78	-0.29	0.05			1 m	133	1.23	-0.06	0.04
	25cm	0.5	62.2	0.49	-0.22	0.05			2 m	149	2.37	-0.19	0.03
	50 cm	0.5	58.0	0.37	-0.40	0.10			3 m	108	1.13	-0.21	0.05
	60cm	0.5	43.0	0.46	-0.26	0.05			4 m	105	1.49	-0.29	0.07
	80 cm	0.5	67.5	1.07	-0.16	0.05			5 m	92.8	0.96	-0.13	0.09
	100 cm	0.5	98.6	0.73	-0.15	0.09			6 m	52.6	0.38	0.15	0.05
Wood	20 cm	12.4	6.68	0.04	-0.29	0.13		Phloem	-5 cm	545	7.05	-0.60	0.08
	25cm	1.81	9.39	0.12	-0.32	0.05			5 m	11.7	0.17	-0.10	0.06
	50 cm	18.9	15.6	0.15	-0.13	0.07							
	60cm	2.35	11.9	0.11	-0.17	0.05							
	80 cm	1.34	28.1	0.38	-0.05	0.05							
	100 cm	0.76	69.9	0.62	-0.50	0.05							
Root	-5 cm	10	81.7	0.95	-0.35	0.05		Root	-5 cm	63.2	0.24	-0.58	0.05
	-15 cm	5	155	1.93	-0.42	0.03			-15 cm	111	0.40	-0.59	0.06
Whole plant		91.96	87.20	70.65	-0.65	0.23							

Table 5. Nickel isotopic fractionation $\Delta^{60}Ni$, calculated between bulk soil and average $\delta^{60}Ni$ in roots, $\Delta^{60}Ni_{bulk\ –root}$, between available Ni and roots, $\Delta^{60}Ni_{available\ –root}$, and between roots and leaves, $\Delta^{60}Ni_{root\text{-}leaf}$. Reported 2σ values were calculated applying the error propagation formulas reported in equation 4.

SR_{150}	$\Delta^{60}Ni_{bulk\ soil\text{-}root}$	2σ	$\Delta^{60}Ni_{available\ -\ root}$	2σ	Plant height	$\Delta^{60}Ni_{root\text{-}leaf}$	2σ
H1	0.21	0.12	0.06	0.12	50cm	0.28	0.08
H2	0.22	0.09	0.24	0.09	60 cm	0.37	0.08
					80 cm	0.40	0.08
					110 cm	0.44	0.08
					150 cm	0.51	0.07
SR_{600}	$\Delta^{60}Ni_{bulk\ -root}$	2σ	$\Delta^{60}Ni_{available\ -\ root}$	2σ	Plant height	$\Delta^{60}Ni_{root\text{-}leaf}$	2σ
H1	0.58	0.08	0.91	0.09	2 m	-0.26	0.08
H2	0.60	0.09	1.11	0.08	3 m	-0.40	0.08
H3			1.21	0.07	4 m	-0.39	0.08
					5 m	-0.29	0.07
					6 m	-0.34	0.11

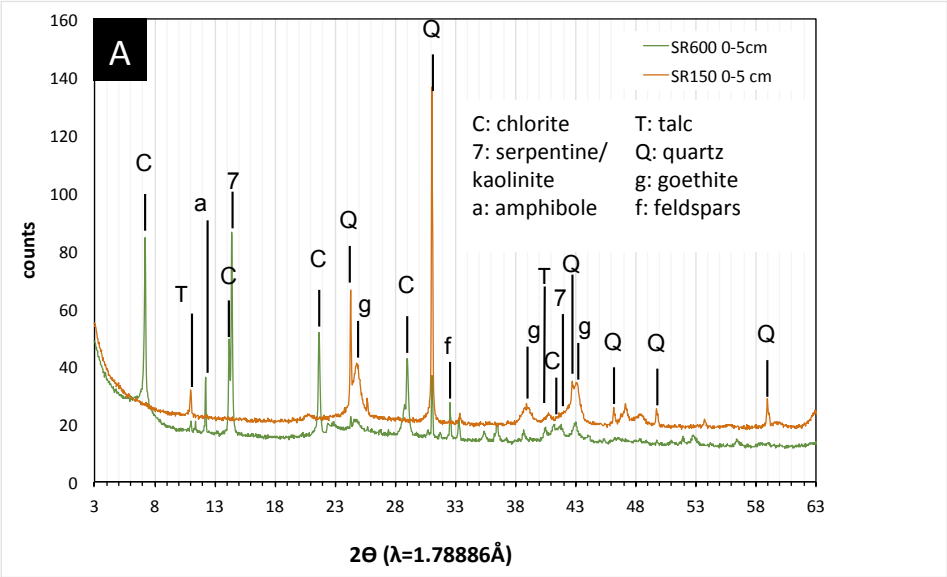

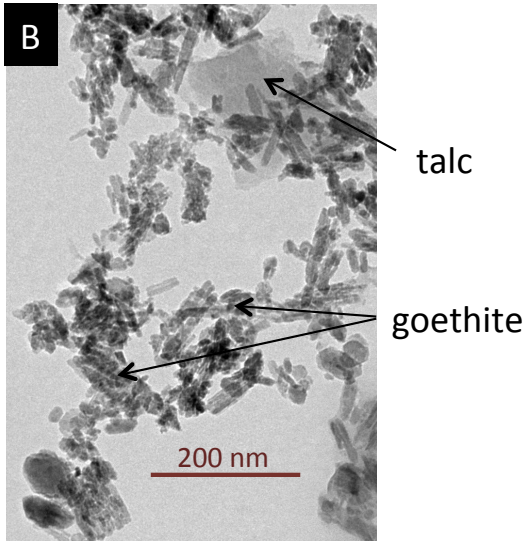

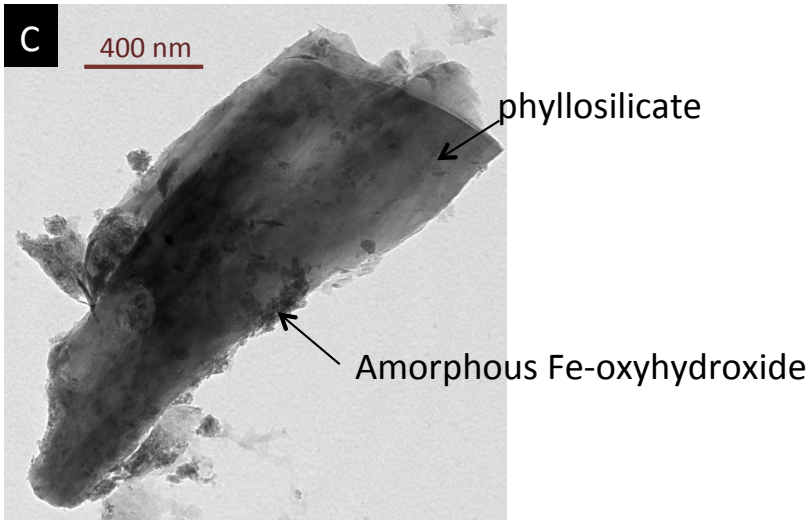

Fig.1 XRD patterns obtained on bulk soils, H1 horizons of SR_{150} and SR_{600} (A). TEM micrographs of the fine fraction <50 µm of SR_{150} (B) and SR_{600} (C) soils, H1 horizons.

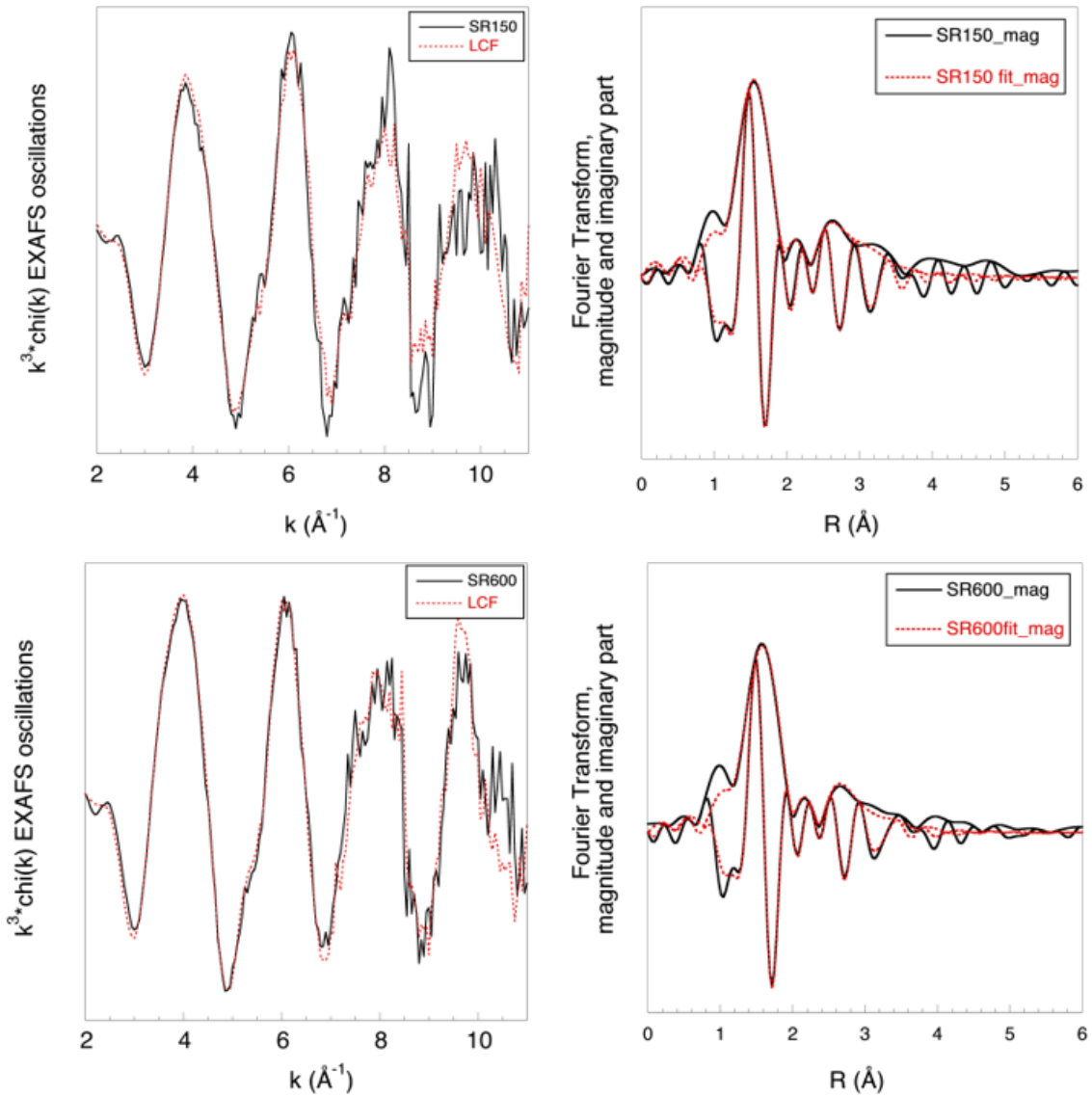

Fig.2 EXAFS oscillations obtained at Ni-K edge, Linear combination fitting (left graphs) and theoretical fitting (or shell by shell fitting, right graphs), for SR_{150} (up) and SR_{600} (down). Fitting parameters are reported in Table 2.

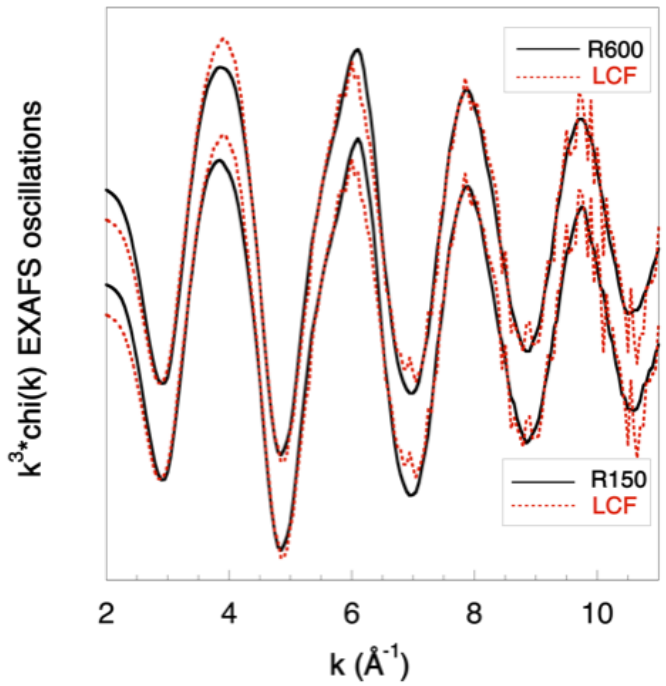

Fig.3 EXAFS oscillations at Ni K edge of *R.*cf. *bengalensis* leaves from R_{150} and R_{600} specimen. Oscillations are fitted as a combination of reference spectra (see Table 3 for fitting parameters).

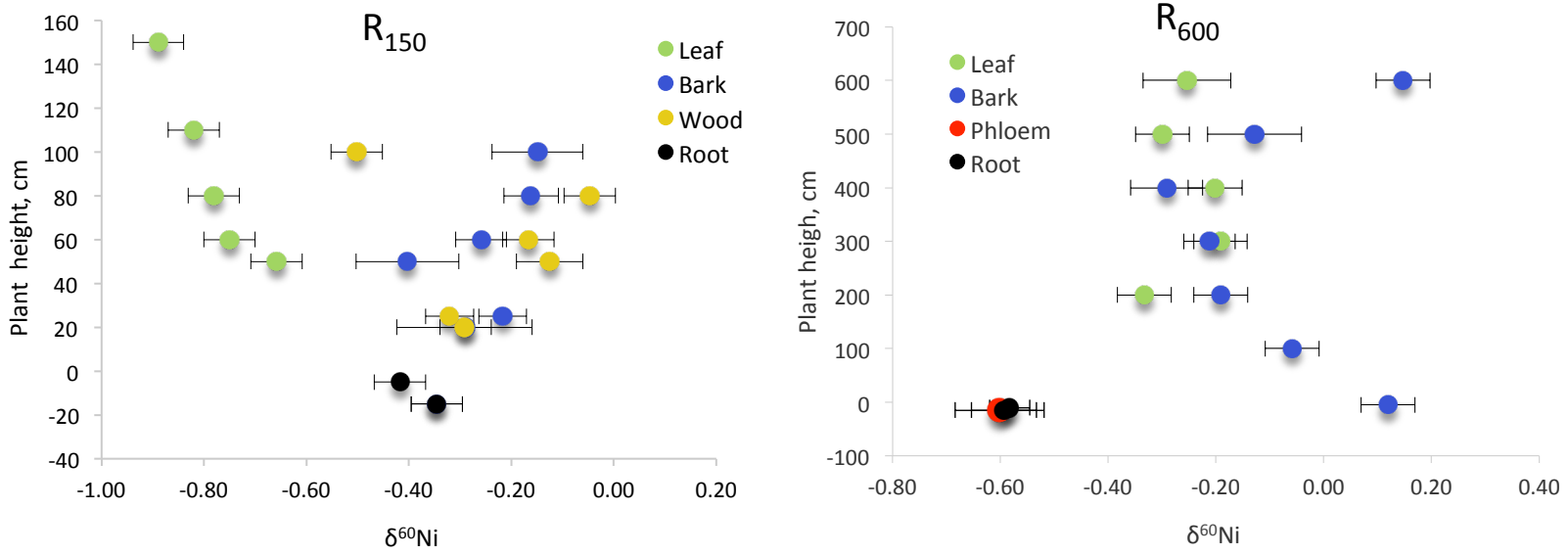

Fig.4 Nickel isotopic composition, δ^{60}Ni, in leaf, root, bark and wood samples of *R.* cf. *bengalensis* specimen R_{150}, and in leaf, bark and phloem tissue samples of the R_{600} specimen. All results are the average of three measurements for each sample and the relative standard deviations correspond to the instrumental error. When the 2σ associated to δ^{60}Ni values are < 0.05 ‰, the value of 2σ = 0.05 ‰ obtained for Oak Leaves reference material V464 (δ^{60}Ni = -0.02 ± 0.05 ‰, N=6) is used.

Table SI 1. Elemental composition of SR_{150} and SR_{600} soil samples in µmol kg^{-1} for trace elements, oxide percentages for major elements and percentage of organic carbon. The range of standard deviation associated to reported results is between 5% and 20% for trace elements (5% for Ni), between 2% and 10% for major and minor elements, and 2 % for organic carbon, as reported by the Service d'Analyse des Roches et des Minéraux, at Centre de Recherches Pétrographiques et Géochimiques, Nancy, France.

µmol kg^{-1} and %	**Cu**	**Pb**	**Sc**	**Co**	**Cr**	**Zn**	**%SiO_2**	**%Al_2O_3**	**%Fe_2O_3**	**%MnO**	**%MgO**	**%CaO**	**%Na_2O**	**%K_2O**	**%TiO_2**	**%C_{org}**
SR_{150} H1 bulk	591	24.71	663	7.46	283	3.59	28.9	4.36	34.0	0.47	1.43	0.49	< d.l.	0.10	0.15	7.44
SR_{150} H2 bulk	556	23.36	773	8.89	364	3.66	30.5	5.15	39.8	0.52	1.61	0.14	< d.l.	0.07	0.18	2.91
SR_{150} H1 >1.5mm	517	24.07	686	7.67	302	3.62	30.2	4.53	35.1	0.48	1.46	0.41	< d.l.	0.09	0.16	/
SR_{150} H1 250 - 50µm	818	33.18	630	6.91	313	3.80	26.7	4.20	31.5	0.43	1.42	0.62	< d.l.	0.10	0.14	/
SR_{150} H1 < 50µm	1037	24.40	598	5.46	206	3.36	34.6	3.80	29.9	0.35	1.16	0.55	< d.l.	0.10	0.14	/
SR_{600} H1 bulk	573	12.79	424	4.65	276	3.95	29.2	4.96	14.6	0.35	10.77	1.06	0.21	0.04	0.20	11.84
SR_{600} H2 bulk	510	13.48	566	6.74	358	4.89	36.9	6.58	19.3	0.51	13.21	1.09	0.28	< d.l.	0.24	3.01
SR_{600} H3 bulk	548	13.70	596	8.39	381	4.70	35.4	7.02	22.1	0.64	13.41	0.97	0.29	< d.l.	0.23	1.64
SR_{600} H1 >1.5mm	586	11.57	463	6.12	296	3.83	31.2	5.40	16.3	0.49	11.48	1.03	0.21	0.04	0.20	/
SR_{600} H1 250 - 50µm	902	28.74	370	2.97	245	3.32	26.5	4.40	11.3	0.24	9.61	1.26	0.22	0.05	0.20	/
SR_{600} H1 < 50µm	1695	41.18	380	2.84	278	3.82	35.8	4.55	10.8	0.24	10.25	1.33	0.28	0.06	0.16	/

<d.l. = below the limit of detection

Table SI 2. Exchangeable cations and total soil cation exchange capacity (CEC mEq per 100 g of soil), determined in bulk samples of different horizons of SR_{150} and SR_{600}.

Soil horizon	Na^{+}	K^{+}	Ca^{2+}	Mg^{2+}	Fe^{3+}	Al^{3+}	Si^{4+}	Ni^{2+}	Total CEC
SR_{150} H1	0.08	0.79	14.4	5.8	<d.l.	<d.l.	1.24	0.30	22.7
SR_{150} H2	0.03	0.24	3.66	2.08	<d.l.	0.07	1.15	0.49	7.72
SR_{600} H1	0.09	0.59	10.0	42.4	<d.l.	<d.l.	1.09	0.38	54.6
SR_{600} H2	0.05	0.17	3.22	20.1	<d.l.	<d.l.	1.15	0.23	24.9
SR_{600} H3	0.05	0.06	1.21	16.1	<d.l.	0.05	1.17	0.12	18.7

<d.l. = below the limit of detection

Table SI 3. Element concentrations (µmol g^{-1}) in leaf, bark, wood and root samples of *R. bengalensis* R_{150} plant. Results are the average of three measurements for each samples. Standard deviation correspond to the triplicate of the measurements.

Tree part	Height	Mg	K	Ca	Mn	Fe	Ni	Zn	Cr	Cu	Co
Leaf	50 cm	132±0.9	483±3.8	749±22.4	12.7±0.14	10.6±0.16	171±1.10	2.56±0.01	0.1±0.01	0.07±0.01	1.78±0.03
	60 cm	131±0.24	459±2.0	785±21.3	12.5±0.06	13.3±13.6	156±0.62	2.83±0.03	0.2±0.01	0.07±0.01	1.74±0.01
	80 cm	85±0.73	516±1.4	621±19.7	10.1±0.02	8.37±0.37	221±16.0	6.73±0.07	0.1±0.01	0.06±0.01	1.59±0.01
	110 cm	139±0.60	366±3.5	691±22	14.8±0.12	10.6±0.85	134±2.40	3.03±0.05	0.1±0.01	0.09±0.01	1.68±0.03
	150 cm	172±1.78	546±6.3	651±31.0	14.8±0.31	9.08±1.85	138±2.75	3.61±0.05	0.1±0.01	0.09±0.01	1.47±0.04
Bark	20 cm	41.5±0.17	244±1.2	1697±38.4	2.0±0.03	19.9±1.16	68.7±0.78	6.76±0.10	0.2±0.01	0.06±0.01	0.18±0.0
	25 cm	41.1±0.12	203±1.2	2093±10.4	2.3±0.01	27.2±0.83	62.1±0.49	7.42±0.06	0.2±0.0	0.09±0.0	0.19±0.0
	40 cm	62.9±0.13	221±2.4	1669±41.6	4.4±0.06	17.6±1.48	58±0.37	3.54±0.07	0.0±0.0	0.11±0.01	0.27±0.01
	60 cm	46.1±0.26	243±1.0	1519±32.4	5.4±0.06	14.5±1.24	43.0±0.46	2.38±0.01	0.0	0.12±0.01	0.24±0.01
	80 cm	71.2±0.03	344±3.3	1404±48.6	3.0±0.04	18±2.15	67.5±1.07	3.69±0.07	0.7±0.64	0.15±0.01	0.23±0.01
	90 cm	107±1.28	507±2.3	1364±25.4	2.01±0.02	15.5±1.42	98.6±0.73	4.43±0.01	0.0±0	0.13±0.73	0.3±0.01
Wood	20 cm	22.6±0.15	128±2.0	333±20.9	0.2±0.01	4.47±0.58	6.7±0.04	0.25	<d.l.	0.02±0	0.02±0.0
	25 cm	22.9±0.13	154±2.8	454±26.1	0.3±0.01	7.48±0.62	9.4±0.12	0.36±0.01	<d.l.	0.05±0.01	0.03±0
	40 cm	34.4±0.08	224±37.3	666±32.9	0.4±0.02	8.96±1.02	15.6±0.15	0.59±0.01	<d.l.	0.08±0.01	0.05±0
	60 cm	36.1±0.37	205±3.2	673±20.2	0.4±0.01	8.14±0.80	11.9±0.11	0.89±0.02	<d.l.	0.04±0.01	0.04±0
	80 cm	47.9±0.66	305±1.7	623±18.3	0.5±0.01	8.16±0.86	28.1±0.38	0.88±0.01	<d.l.	0.20±0.02	0.07±0.0
	100 cm	65.7±0.30	412±3.3	629±34.1	0.8±0.02	10.0±1.08	69.9±0.62	1.67±0.02	<d.l.	0.20±0.02	0.16±0.0
Root	-5 cm	99.1±1.25	237±2.7	963±31.7	4.5±0.04	44.2±1.66	154±1.93	2.07±0.03	0.8±0.01	0.06±0.0	0.38±0.0
	-15 cm	85.7±0.66	155±1.4	414±16.4	3.2±0.05	169±2.78	81.7±0.95	2.37±0.02	4.1±0.35	0.07±0.0	0.47±0.01

<d.l. = below the limit of detection

Table SI 4. Element concentrations (µmol g^{-1}) in leaf, bark, and phloem samples of *R. bengalensis* R_{600} plant. Results are the average of three measurements for each samples. Standard deviation correspond to the triplicate of the measurements.

Tree part	Height	Mg	K	Ca	Mn	Fe	Ni	Zn	Cr	Cu	Co
Leaf	2m	149±0.75	684±10.7	995±36.8	1.98±0.03	9.99 ±1.18	522±7.83	3.76±0	0.06±0.01	0.05±0.01	0.32±0.01
	3m	183±1.42	463±3.37	923±22.1	1.83±0.02	8.93±0.44	349±5.50	2.15±0	0.09±0.01	0.05±0.0	0.19±0.01
	4m	144±1.77	552±13.7	854±28.3	1.86±0.03	8.95±0.80	309±5.94	1.31±0.01	0.07±0.00	0.06±0.0	0.20±0.0
	5m	209±3.22	686±21.5	1180±221	1.86±0.11	20.2±7.51	220±6.85	2.13±0.01	0.21±0.15	<d.l.	0.12±0.02
	6m	97±0.93	436±26.5	873±151	2.15±0.02	13.7±2.02	156±1.17	1.15±0.01	0.21±0.05	<d.l.	0.17±0.01
Bark	1m	36±0.22	278±3.95	1565±35.7	0.53±0.01	14.2±0.45	133±1.23	1.94±0.0	0.02±0.00	0.06±0.01	0.03±0
	2m	33±0.37	305±4.98	1544±25.2	0.66±0.02	14.1±0.68	149±2.37	1.60±0.0	0.02±0.0	0.05±0.01	0.04±0
	3m	33±0.18	287±4.81	1486±35.1	0.71±0.01	14.2±1.42	108±1.13	0.66±0.0	0.01±0.0	0.07±0.01	0.04±0
	4m	33±0.37	450±4.62	1553±14.8	1.49±0.01	14.0±0.5	105±1.49	0.87±0.0	0.01±0.0	0.07±0.0	0.08±0
	5m	50±0.47	293±6.26	1770±39.2	2.21±0.02	16.4±0.9	93±0.96	1.40±0.0	0.01±0.0	0.08±0.0	0.10±0
	6m	78±0.30	155±1.22	742±23.3	0.49±0.0	6.8±0.5	53±0.38	0.78±0.0	0.01±0.0	0.03±0.02	0.02±0
Phloem	-5 cm	127.1±0.74	510±5.22	1488±35.1	10.6±0.09	16.33±1.09	545±7.05	19.4±0.02	0.26±0.01	0±0	0.6±0
	5 m	71±0.76	344±10.4	580±79.0	0.39±0.04	3.50±2.97	12±0.24	0.09±0.00	0.01±0.01	0.07±0.03	0.02±0
Root	-5 cm	91.2±1.09	228±3.40	301±12.9	1.37±0.01	22.3±0.38	63.2±0.24	3.03±0.01	1.50±0.07	0.11±0.0	0.09±0
	-15 cm	186±0.61	188±10.4	447±232	2.60±0.08	41.9±8.77	111±0.4	5.57±0.00	4.35±0.07	0.22±0.08	0.17±0.01

<d.l. = below the limit of detection

Notes

The concentrations of Ca and K in the plant material are relatively high compared to the amount of exchangeable cations in the corresponding soils. In both plants, the highest Ca concentration is in the bark, where it reaches 2000 µmol g^{-1} and 1700 µmol g^{-1} in R_{150} and R_{600}, respectively. The highest K concentrations is recorded in the leaves, 546 µmol g^{-1} in R_{150} and 686 µmol g^{-1} R_{600}. Despite the fact that exchangeable Mg in the soil is 10-fold higher in SR_{600} than in SR_{150}, Mg concentrations are similar in both plants, *e.g.* ~150 µmol g^{-1} in the leaves. Other elemental concentrations, such as Fe, Mn, Cu and Zn are in the ranges previously reported for *R. bengalensis*(van der Ent et al., 2017).

Some clear trends are found in R_{150}, the Mg and K concentrations in the bark and wood increase with height, from the bottom to the top. This trend is also observed for Mg in bark of R_{600}, but no trend is observed for K. For the trace elements no clear trends is found. Cobalt is more concentrated in R_{150} leaves than in R_{600} leaves, although Co contents in SR_{150} and SR_{600} soils are in the same range of order.

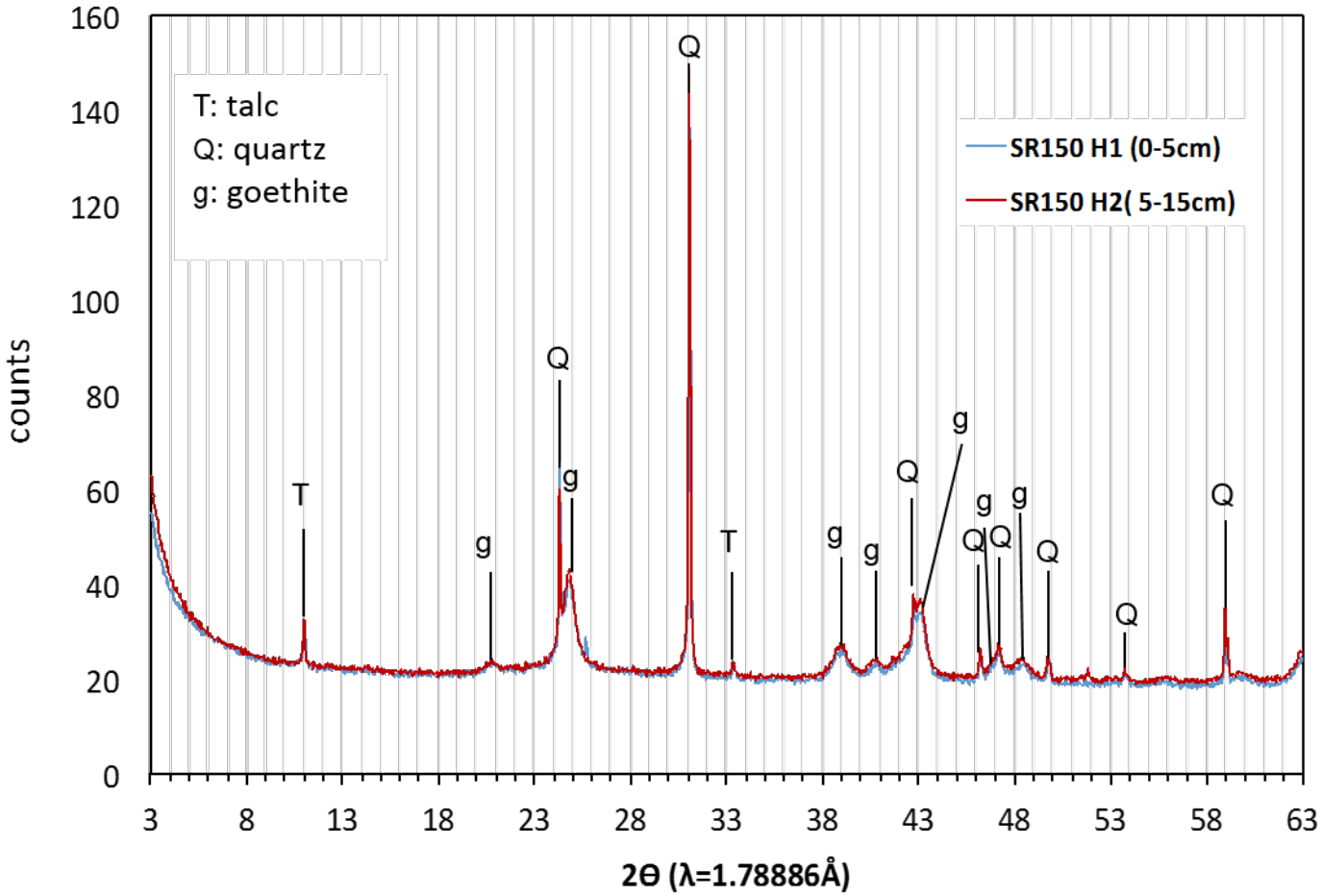

Figure SI 1. XRD patterns obtained on SR_{150} bulk soil, horizon H1 (0-5 cm) and H2 (5-15 cm). The pattern demonstrates the predominance of goethite and quartz, associated to one phyllosilicate (talc), no clay minerals or other silicate could be evidenced.

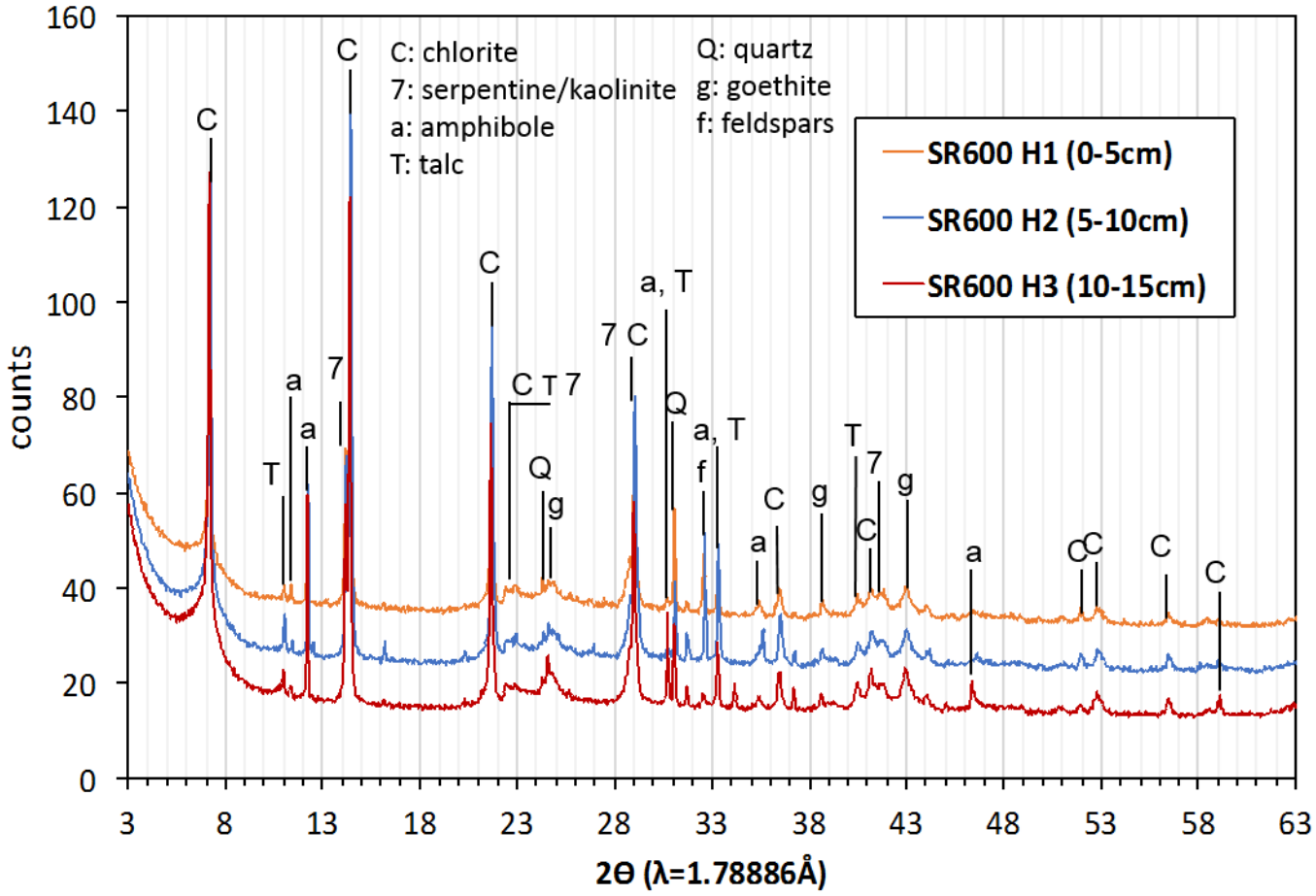

Figure SI 2. XRD patterns obtained on SR_{600} bulk soil, horizon H1 (0-5 cm), H2 (5-10 cm) and H3 (10-15 cm). The patterns evidence a predominance of phyllosilicates, chlorite, talc and 7Å phyllosilicate (serpentine or kaolinite). Primary minerals such as amphibole and feldspars were also detected. Quartz and goethite appear as minor phases.

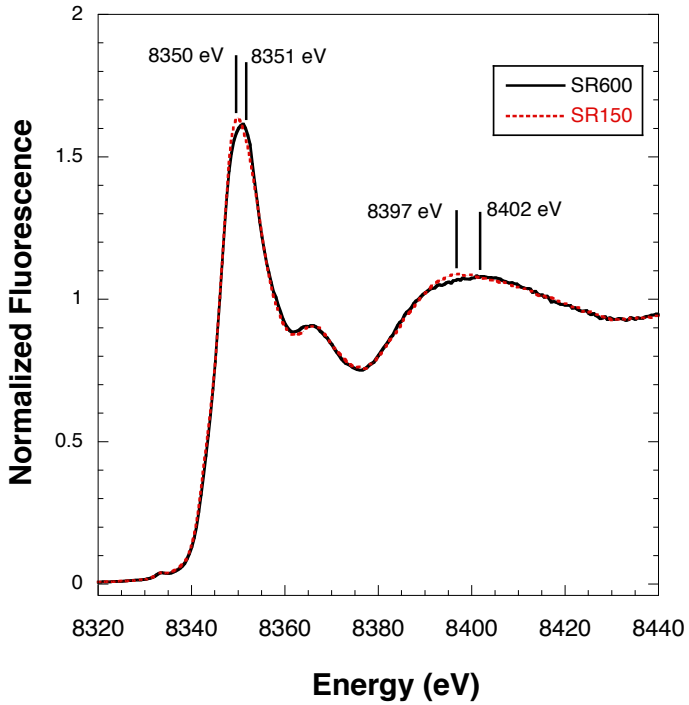

Figure SI 3. XANES spectra at Ni-K edge from SR_{150} and SR_{600} soils (surface horizon H1, bulk soil samples).

References

van der Ent, A., Callahan, D. L., Noller, B. N., Mesjasz-Przybylowicz, J., Przybylowicz, W., Barnabas, A., & Harris, H. H. (2017). Nickel biopathways in tropical nickel hyperaccumulating trees from Sabah (Malaysia). *Scientific Reports*, *7*. https://doi.org/DOI: 10.1038/srep41861